7 Reweighting methods

7.1 BACKGROUND

7.1.1 Distribution functions

One longstanding limitation on the resolution of Monte Carlo simulations near phase transitions has been the need to perform many runs to precisely characterize peaks in response functions such as the specific heat. Dramatic improvements have become possible with the realization that entire distributions of properties, not just mean values, can be useful; in particular, they can be used to predict the behavior of the system at a temperature other than that at which the simulation was performed. There are several different ways in which this may be done. The reweighting may be done after a simulation is complete or it may become an integral part of the simulation process itself. The fundamental basis for this approach is the realization that the properties of the systems will be determined by a distribution function in an appropriate ensemble. Thus, in the canonical ensemble, for example, the probability of observing a particular state in a simple Ising ferromagnet with interaction constant $\mathcal{J}$ at temperature T is proportional to the Boltzmann weight, $\exp(-KE)$ where we define $K = \mathcal{J}/k_{\mathrm{B}}T$ as the dimensionless coupling. The probability of simultaneously observing the system with total (dimensionless) energy $E = -\sum \sigma_i \sigma_j$ and total magnetization $M = \sum \sigma_i$ is then

$$P_K(E, M) = \frac{W(E, M)}{Z(K)} \exp(-KE), \tag{7.1}$$

where $W(E, M)$ is the number of configurations (density of states) with energy E and magnetization M, and $Z(K)$ is the partition function of the system. Thus, the density of states contains all the relevant information about the systems and the effect of temperature can be straightforwardly included.

7.1.2 Umbrella sampling

In the following discussion we follow Frenkel and Smit (1996) by introducing the 'overlapping distribution method' (Bennett, 1976) for the estimation of the free energy difference ΔF between two systems, labeled 0 and 1, with partition functions Z_0 and Z_1. At this point, we consider off-lattice systems with N particles in a volume V at the same inverse temperature β (but differing in

some other property, e.g. systems in different phases, or with some parameter in the Hamiltonian being different). The free energy difference can then be written as ($\beta \equiv 1/k_B T$)

$$\begin{aligned}\beta \Delta F &= -\ln(Z_1/Z_0) \\ &= -\ln\left(\int d\mathbf{r}^N \exp[-\beta U_1(\mathbf{r}^N)] \Big/ \int d\mathbf{r}^N \exp[-\beta U_0(\mathbf{r}^N)]\right), \end{aligned} \tag{7.2}$$

where $\mathbf{r}^N$ stands symbolically for the set of coordinates $\{\mathbf{r}_1, \mathbf{r}_2, \ldots, \mathbf{r}_N\}$ of the N particles, and U_0, U_1 are the potential energies of the two systems.

Suppose that a Monte Carlo sampling of the configuration space of system 1 is carried out. For every configuration ($\mathbf{r}^N$) of system 1 generated in this process the potential energy $U_0(\mathbf{r}^N)$ of the system 0 can be computed, and hence $\Delta U \equiv U_1(\mathbf{r}^N) - U_0(\mathbf{r}^N)$ can be obtained for every configuration. We use this information to generate a histogram that is proportional to the probability density $p_1(\Delta U)$ that this energy difference ΔU is observed,

$$p_1(\Delta U) = \int d\mathbf{r}^N \exp(-\beta U_1)\delta(U_1 - U_0 - \Delta U)/Z_1. \tag{7.3}$$

Substituting $U_1 = U_0 + \Delta U$ in the argument of the exponential function, we find

$$\begin{aligned} p_1(\Delta U) &= \exp(-\beta \Delta U) \int d\mathbf{r}^N \exp(-\beta U_0)\, \delta(U_1 - U_0 - \Delta U) \Big/ Z_1, \\ &= \frac{Z_0}{Z_1} \exp(-\beta \Delta U)\, p_0(\Delta U), \end{aligned} \tag{7.4}$$

where

$$p_0(\Delta U) = \int d\mathbf{r}^N \exp(-\beta U_0)\, \delta(U_1 - U_0 - \Delta U) \Big/ Z_0 \tag{7.5}$$

is nothing but the probability density to find the same potential energy difference ΔU between systems 1 and 0 in a Boltzmann sampling of the configurations of system 0. Combining Eqns. (7.2) and (7.4) we readily obtain

$$\begin{aligned} \ln p_1(\Delta U) &= \ln(Z_0/Z_1) - \beta \Delta U + \ln p_0(\Delta U) \\ &= \beta(\Delta F - \Delta U) + \ln p_0(\Delta U). \end{aligned} \tag{7.6}$$

Thus, if there is a range of values ΔU where both $p_1(\Delta U)$ and $p_0(\Delta U)$ can be estimated from two separate simulations, one for system 0 and one for system 1, one can try to obtain $\beta \Delta F$ from a fit of Eqn. (7.6) to the difference between $\ln p_0(\Delta U)$ and $[\beta \Delta U + \ln p_1(\Delta U)]$.

The sampling of the chemical potential $\mu_{ex} \equiv \mu - \mu_{id}(V)$ ($\mu_{id}(V)$ being the chemical potential of an ideal gas of N particles at temperature T in a volume V) can be understood readily in the following way (see the discussion on particle insertion/removal techniques in Chapter 6). We simply assume that

system 1 has N interacting particles while system 0 contains $N-1$ interacting particles and one non-interacting ideal gas particle. This yields (Shing and Gubbins, 1983)

$$\mu_{\mathrm{ex}} = \ln P_1(\Delta U) - \ln P_0(\Delta U) + \beta \Delta U. \tag{7.7}$$

Since Eqn. (7.6) can also be written as

$$P_1(\Delta U) = P_0(\Delta U)\exp[\beta(\Delta F - \Delta U)], \tag{7.8}$$

we conclude that, in principle, knowledge of either $p_1(\Delta U)$ or $p_0(\Delta U)$ suffices to fix ΔF, since these probabilities are normalized, i.e. $\int_{-\infty}^{+\infty} p_1(\Delta U)d(\Delta U) = 1$, $\int_{-\infty}^{+\infty} p_0(\Delta U)\Delta U = 1$. Hence

$$1 = \int_{-\infty}^{+\infty} p_0(\Delta U)\exp[\beta(\Delta F - \Delta U)]d(\Delta U) = \exp(\beta \Delta F)\langle \exp(-\beta \Delta U)\rangle_0. \tag{7.9}$$

Thus, in principle 'only' the factor $\exp(-\beta\Delta U)$ in the system 0 needs to be sampled. However, this result already clearly reveals the pitfall of this method: for the 'typical' configurations of system 0 the difference $\Delta U \propto N$ and hence $\exp(-\beta\Delta U)$ is very small, while larger contributions to this average may come from regions of phase space where $p_0(\Delta U)$ is not so small. As a result, the statistical accuracy of any estimate of ΔF based on Eqn. (7.9) can be very poor.

Torrie and Valleau (1977) attempted to cure this problem by a scheme called 'umbrella sampling'. The basic idea is to improve the accuracy of the estimation of the average in Eqn. (7.9) by modifying the Markov chain that is constructed in the sampling in such a way that one samples both the part of configuration space accessible to system 1 and the part accessible to system 0. This is achieved by replacing the Boltzmann factor of the system by a (non-negative) weight function $\pi(\mathbf{r}^N)$. Using such a weight, and remembering that $\Delta U \equiv U_1(\mathbf{r}^N) - U_0(\mathbf{r}^N)$, the desired average can be rewritten as

$$\begin{aligned}
\exp(-\beta \Delta F) &= \int_{-\infty}^{+\infty} d\mathbf{r}^N(-\beta U_1) \Big/ \int_{-\infty}^{+\infty} d\mathbf{r}^N \exp(-\beta U_0) \\
&= \int_{-\infty}^{+\infty} d\mathbf{r}^N \pi(\mathbf{r}^N)[\exp(-\beta U_1)/\pi(\mathbf{r}^N)] \Big/ \int_{-\infty}^{+\infty} d\mathbf{r}^N \pi(\mathbf{r}^N) \\
&\quad \times [\exp(-\beta U_0)/\pi(\mathbf{r}^N)].
\end{aligned} \tag{7.10}$$

With the notation $\langle \cdots \rangle_\pi$ to denote an average over a probability distribution $\pi(\mathbf{r}^N)$ one obtains

$$\exp(-\beta \Delta F) = \langle \exp(-\beta U_1)/\pi \rangle_\pi / \langle \exp(-\beta U_0)/\pi \rangle_\pi. \tag{7.11}$$

The distribution π must have an appreciable overlap with both the regions of configuration space that are sampled by system 0 and by system 1, in order

that both the numerator and the denominator in Eqn. (7.11) are meaningful. This 'bridging' property of π is alluded to in the name 'umbrella sampling'.

Of course, a drawback of the method is that π is not known a priori; rather one has to construct it using information about the Boltzmann weights of the two systems. It may also be advantageous not to bridge all the way from system 0 to system 1 with a single overlapping distribution, but actually it may be better to perform several 'umbrella sampling' runs in partially overlapping regions. This formulation of the method actually is closely related in spirit to the 'multicanonical sampling', see Section 7.5.

Umbrella sampling has been used to determine absolute values of the free energy in two-dimensional and three-dimensional Ising models by Mon (1985). In two dimensions the nearest neighbor Ising ferromagnet was considered in two different situations: on a $2L \times 2L$ square lattice with periodic boundary conditions (and Hamiltonian $\mathcal{H}_{2L}$), and with the lattice divided up into four separate $L \times L$ square lattices, each with periodic boundaries (and composite Hamiltonian $\overline{\mathcal{H}}_L$). The free energy difference is then

$$f_{2L} - f_L = \frac{\ln\langle \exp[-\beta(\overline{\mathcal{H}}_L - \mathcal{H}_{2L})]\rangle_{\mathcal{H}_{2L}}}{4L^2}. \tag{7.12}$$

For three dimensions this difference can then be evaluated by umbrella sampling by simulating a series of systems with Hamiltonian

$$H' = a\mathcal{H}_{2L} - b\overline{\mathcal{H}}_L, \tag{7.13}$$

where a and b vary from 0 to 1 with $a + b = 1$. The result in two dimensions agrees quite well with the exact value and in three dimensions very precise values were obtained for both simple cubic and body centered cubic models.

A very efficient implementation of umbrella sampling for gas–liquid systems or binary liquid mixtures, where errors resulting from this method can be estimated precisely, has been introduced by Virnau and Müller (2004) under the name of 'Successive Umbrella Sampling'.

7.2 SINGLE HISTOGRAM METHOD

The idea of using histograms to extract information from Monte Carlo simulations is not new, but it was a number of years before it was applied with success to the study of critical phenomena (Ferrenberg and Swendsen, 1988; Ferrenberg, 1991). Here we provide a brief description of the method and show some characteristic analyses.

We first consider a Monte Carlo simulation performed at $T = T_o$, which generates system configurations with a frequency proportional to the Boltzmann weight, $\exp[-K_o E]$. Because the simulation generates configurations according to the equilibrium probability distribution, a histogram $H(E, M)$ of energy and magnetization values provides an estimate for the equilibrium probability distribution; this estimate becomes exact in the limit of an infinite-length run. For a real simulation, the histogram will suffer from statistical

errors, but $H(E, M)/N$, where N is the number of measurements made, still provides an estimate for $P_{K_o}(E, M)$ over the range of E and M values generated during the simulation. Thus

$$H(E, M) = \frac{N}{Z(K_o)} \tilde{W}(E, M) e^{-K_o E}, \tag{7.14}$$

where $\tilde{W}(E, M)$ is an estimate for the true density of states $\tilde{W}(E, M)$. Knowledge of the exact distribution at one value of K is thus sufficient to determine it for any K. From the histogram $H(E, M)$, we can invert Eqn. (7.14) to determine $\tilde{W}(E, M)$:

$$\tilde{W}(E, M) = \frac{Z(K_o)}{N} H(E, M) e^{K_o E}. \tag{7.15}$$

If we now replace $W(E, M)$ in Eqn. (7.1) with the expression for $\tilde{W}(E, M)$ from Eqn. (7.15), and normalize the distribution, we find that the relationship between the histogram measured at $K = K_o$ and the (estimated) probability distribution for arbitrary K is

$$P_K(E, M) = \frac{H(E, M) e^{\Delta K E}}{\sum H(E, M) e^{\Delta K E}} \tag{7.16}$$

with $\Delta K = (K_o - K)$. From $P_k(E, M)$, the average value of any function of E and M, denoted $f(E, M)$, can be calculated as a continuous function of K:

$$\langle f(E, M) \rangle_K = \sum f(E, M) P_K(E, M). \tag{7.17}$$

The ability to continuously vary K makes the histogram method ideal for locating peaks, which occur at different locations, in different thermodynamic derivatives, and provides the opportunity to study critical behavior with unprecedented resolution.

7.2.1 The Ising model as a case study

As an example of the implementation of this method, we shall now discuss results for the three-dimensional ferromagnetic Ising model. We remind the reader that the Hamiltonian is

$$\mathcal{H} = -\mathcal{J} \sum_{\langle i,j \rangle} \sigma_i \sigma_j, \tag{7.18}$$

where the spins σ_i, σ_j take on the values ± 1 and the sum is over all nearest neighbor pairs. As we saw in Chapter 4, in a finite system the phase transition is rounded and shifted from its infinite lattice location (Eqn. (4.13)). If one looks closely one sees that the difference between the true critical temperature and a 'pseudocritical' temperature of the finite system (estimated e.g. from the specific heat maximum) is not simply given by a power of L but rather includes correction terms as well. Obviously, great resolution is needed if these correction terms are to be included properly. We use this Ising model as

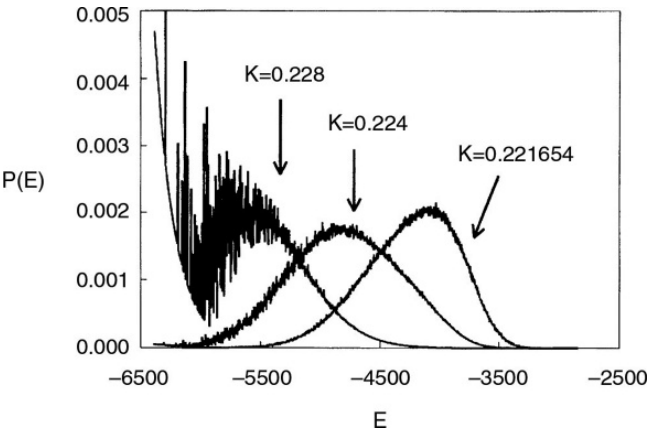

Fig. 7.1 Probability distribution of the dimensionless energy E for $L = 16$. The data from the simulation were obtained at $K_o = 0.221\,654$; the other distributions come from reweighting as described in the text. From Ferrenberg and Landau (1991).

an example to demonstrate the manner in which an accurate analysis can be carried out.

A detailed Monte Carlo study was made for $L \times L \times L$ simple cubic lattices with fully periodic boundary conditions (Ferrenberg and Landau, 1991). Most of the simulations were performed at $K_o = 0.221\,654$, an earlier estimate for the critical coupling K_c obtained by a Monte Carlo renormalization group (MCRG) analysis (Pawley *et al.*, 1984) of the kind which will be described in Chapter 9. Data were obtained for lattices with $8 \leq L \leq 96$, and between 3×10^6 and 1.2×10^7 MCS and measurements were made at intervals of either 5 or 10 MCS after up to 10^5 MCS were discarded for equilibrium. (For the largest lattice, the total run length was more than 5000 times the relevant correlation time τ (Wansleben and Landau, 1991), with τ determined as described in Chapter 4.) Error estimates were obtained by dividing the data from each simulation into a set of between 5 and 11 statistical samples (bins) and considering the distribution of values obtained from each bin. Because each histogram is used to determine multiple quantities, some correlations are expected between the different results; however, these were found to be smaller than the statistical errors, and the individual errors could thus be treated as uncorrelated. An analysis was performed for bins of different sizes choosing the final bin sizes so that systematic errors were negligible compared to the statistical error.

Sufficiently far from K_o the histogram method yielded values which are obviously wrong, because in the range of E that is then required the histogram has so few entries that the method has broken down. As K is varied, the peak in the reweighted distribution moves away from that of the measured histogram and into the 'wings' where the statistical uncertainty is high, thus leading to unreliable results. This is because of the finite range of E and M generated in a simulation of finite length as well as the finite precision of the individual histogram entries. This problem is demonstrated in Fig. 7.1, which shows the normalized (total) energy histogram for the $L = 16$ lattice measured at $K_o = 0.221\,654$ along with the probability distributions for two additional couplings

($K = 0.224$ and $K = 0.228$) calculated by reweighting this histogram. The calculated distribution for $K = 0.224$ is fairly smooth, although the right side of the distribution, which occurs closer to the peak of the measured histogram, is clearly smoother than the left side. The 'thickening' of the distribution on the side in the tail of the measured histogram is an indication that the statistical errors are becoming amplified and that the extrapolation is close to its limit of reliability. The distribution calculated for $K = 0.228$ is clearly unreliable. This limitation in ΔK must always be kept in mind, particularly for large systems, because the reliable range of K values decreases as the system size increases.

In the critical region a simple histogram covers a finite fraction of the required region in finite size scaling irrespective of size. By performing a small number of additional simulations at different values of K we can guarantee that the results obtained from the single-histogram equation do not suffer from systematic errors. These were done for $L = 32$ at $K_o = 0.2215$, and the location and value of the peaks in the thermodynamic derivatives were determined. Simulations were also performed using two different sets of the random number generator 'magic numbers'. Within the observed statistical errors, no systematic deviations are present. A further test for systematic errors is to use the histogram measured at $K_o = 0.221\,654$ to predict the behavior of the system at $K = 0.2215$ and then compare the results with those obtained directly from the simulation performed at $K_o = 0.2215$. The reweighted results agreed, within the calculated error, with the directly measured results for all quantities except the specific heat (which also agreed to within 2σ).

As described previously (Chapter 4), the critical exponent ν can be estimated without any consideration of the critical coupling K_c. For sufficiently large systems it should be possible to ignore the correction term so that linear fits of the logarithm of the derivatives as a function of $\ln L$ provide estimates for $1/\nu$. In fact, $L_{min} = 24$ was the smallest value that could be used except in the case of the derivative of the magnetization cumulant where linear fits are still satisfactory for $L_{min} = 12$. Combining all three estimates, the analysis yielded $1/\nu = 1.594(4)$ or $\nu = 0.627(2)$. By adding a correction term, data from smaller systems can be included. Fits were made of the derivatives to Eqn. (4.14) by fixing the values of ν and ω, determining the values of a and b which minimize the χ^2 of the fit and then repeating the procedure for different values of ν and ω. The errors are correlated and the minimum in χ^2 is quite shallow. Scans over a region of (ν, ω) space for the different quantities revealed the global minimum where $\nu = 0.6289(8)$.

Once there is an accurate value for ν, K_c can be estimated quite accurately. As discussed in Chapter 4, the locations of the maxima of various thermodynamic derivatives provide estimates for effective transition couplings $K_c(L)$ which scale with system size like Eqn. (4.13). These estimates for $K_c(L)$ are plotted as a function of L for $L < 96$ in Fig. 7.2. The solid lines are second order polynomial fits to the data and are drawn to guide the eye. The specific heat peaks (open circles in Fig. 7.2), which occur further from the simulated temperature than any other quantity considered here, fall just *outside the range of validity* of the histogram analysis, especially for $L = 96$. This systematic

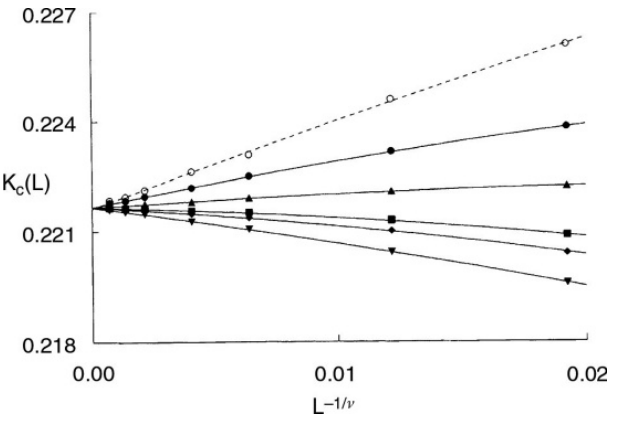

Fig. 7.2 Size dependence of the finite-lattice effective couplings temperatures for the three-dimensional Ising model. The symbols represent the data while the lines (dashed for the specific heat and solid for the other quantities) are fits to Eqn. (7.3) with $\nu = 0.6289$ and including the correction term. From Ferrenberg and Landau (1991).

underestimation of the error, particularly pronounced for $L = 96$, can be compensated for by either increasing the error values, or by removing the $L = 96$ result. In either case, the estimate for K_c is in agreement with that from the other quantities but the error bar is much larger. The result for the derivative of m on the $L = 96$ system is just at the limit of reliability for the histogram analysis. There is noticeable curvature in the lines in Fig. 7.2 indicating that corrections to scaling are important for the smaller systems. If only the results for $L \geq 24$ are analyzed, linear fits to Eqn. (4.13), with no correction terms are obtained; i.e. for sufficiently large L, K_c should extrapolate linearly with $L^{-1/\nu}$ to K_c. Figure 7.2 shows noticeable curvature for small system sizes so corrections must be included; these produce estimates for ω and K for each of the quantities which yield a value $K_c = 0.221\ 659\ 5(26)$. The values of the correction exponent are again consistent with $\omega = 1$ except for the finite-lattice susceptibility (which has the smallest correction term). Fits performed by allowing both ω and ν to vary yield consistent estimates for ν and K_c but with larger errors due to the reduced number of degrees of freedom of the fit.

The finite size scaling analysis was repeated using corrections to scaling and the theoretically predicted forms with $\omega = 1$ and the re-analysis of all thermodynamic derivatives yielded $\nu = 0.6294(2)$. While the statistical error in these values was small, the χ^2 of the fit, as a function of $1/\nu$, has a broad shallow minimum so that the actual statistical error, calculated by performing a true non-linear fit, would be larger. Unfortunately, neither the resolution nor the number of different lattice sizes allows such a fit. With this value of ν, K_c was estimated as $K_c = 0.221\ 6574(18)$, which is in excellent agreement with the previous estimate.

Finite size scaling can also be used to estimate other exponents from bulk properties at K_c. The value of ν which was obtained from the derivative of the magnetization cumulant and the logarithmic derivatives of m and m^2 at K_c

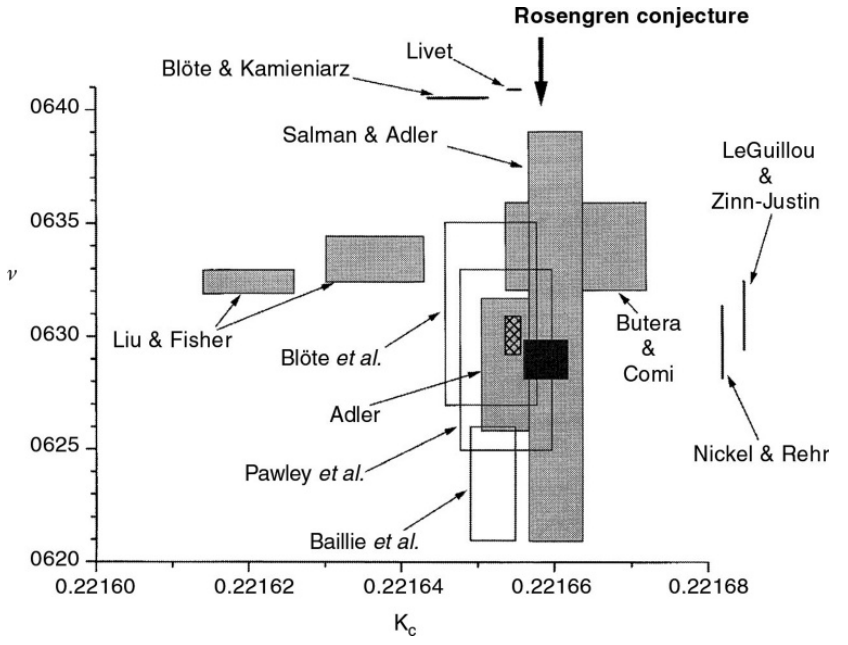

Fig. 7.3 High resolution estimates for K_c and ν for the simple cubic Ising model (boxes show estimates including errors bars; horizontal and vertical lines show the range of independent estimates for only one parameter): series expansions (Adler, 1983; Liu and Fisher, 1989; Nickel and Rehr, 1990; Butera and Comi, 1997; Salman and Adler, 1998), Monte Carlo renormalization group (Pawley *et al.*, 1984; Blöte *et al.*, 1989a,b; Baillie *et al.*, 1992), ε-expansion renormalization group (LeGuillou and Zinn-Justin, 1980), Monte Carlo (Livet, 1991; Blöte and Kamieniarz, 1993). The highest resolution studies, combining Monte Carlo with finite size scaling, are shown by the solid box (Ferrenberg and Landau, 1991) and the cross-hatched box (Blöte *et al.*, 1995). The Rosengren conjecture (Rosengren, 1986) is shown by the vertical arrow.

is identical to that obtained by scaling the maximum value of the derivatives. The scaling behavior of m at K_c yields $\beta/\nu = 0.518(7)$. (The linear fit for $L > 24$ yields $\beta/\nu = 0.505$.) Combining this value for β/ν with the estimate for ν, we obtain $\beta = 0.3258(44)$ which agrees with the ε-expansion result 0.3270(15). Estimates for γ/ν could be extracted from the scaling behavior of the finite-lattice susceptibility yielding $\gamma/\nu = 1.9828(57)$ or $\gamma = 1.2470(39)$ or from the true susceptibility at K_c which gave $\gamma/\nu = 1.970(11)$ or $\gamma = 1.2390(71)$, in excellent agreement with the ε-expansion value of 1.2390(25).

In Fig. 7.3 we show the results of this Monte Carlo study as well as other high resolution simultaneous estimates for ν and K_c. The boxes present the quoted error bars in both K_c and ν assuming independent errors. To the best of our knowledge, all error estimates represent 1 standard deviation. The results from the Monte Carlo study are represented by the filled box and agree well with some MCRG results (Pawley *et al.*, 1984; Blöte *et al.*, 1989a,b), but are outside the error bars of Baillie *et al.* (1992), which in turn have only tenuous overlap with the other MCRG values. The value for ν is also consistent with the ε-expansion result (LeGuillou and Zinn-Justin, 1980) and some of the series expansion results (Adler, 1983; Nickel and Rehr, 1990) but disagrees with others (Liu and Fisher, 1989), which also disagree with the other series

values. Transfer matrix Monte Carlo results (Nightingale and Blöte, 1988) yield $\nu = 0.631$ with errors of either 0.006 or 0.002 depending on the range of sizes considered in the analysis and a numerical lower bound (Novotny, 1991), $\nu = 0.6302$ falls within 2σ of the result. Other estimates for K_c (Livet, 1991; Blöte *et al.*, 1995), obtained by assuming fixed values for ν, also lie outside these error bars. The estimate for K_c derived from the maximum slope of m differs substantially from that obtained from the other quantities, although it does agree within 2 standard deviations. If we remove it from the analysis, this estimate for K_c drops to 0.221 657 6(22), which is in even better agreement with the other values presented above. Clearly the question of precise error bar determination remains for all of these numerical methods.

In another high resolution study (Blöte *et al.*, 1995) high statistics runs were made on many, smaller systems and the finite size scaling behavior was carefully examined. Corrections were found beyond those caused by the leading irrelevant scaling field, and with the inclusion of correction exponents from renormalization group theory the critical point was estimated to be at $K_c = 0.221\,654\,6(10)$.

Why do we expend so much effort to locate K_c? In addition to testing the limits of the method, one can also test the validity of a conjectured closed form for K_c (Rosengren, 1986) obtained by attempting to generalize the combinatorial solution of the two-dimensional Ising model to three dimensions:

$$\tanh K_c = \left(\sqrt{5} - 2\right) \cos(\pi/8). \tag{7.19}$$

This relation gives $K_c = 0.221\,658\,63$, which agrees rather well with current best estimates. However, Fisher (1995) argued quite convincingly that this conjecture is not unique and most probably not valid.

The combination of high statistics Monte Carlo simulations of large systems, careful selection of measured quantities, and use of histogram techniques yields results at least as good as those obtained by any other method. All of the analysis techniques used here are applicable if yet higher quality data are obtained and should help define the corrections to scaling. (These same techniques have also been used to provide very high resolution results for a continuous spin model, the three-dimensional classical Heisenberg model (Chen *et al.*, 1993). The size of the error bars on current estimates for K_c indicate that even higher resolution will be required in order to unambiguously test the correctness of the conjectured 'exact' value for K_c. Further improvement will require substantially better data for some of the larger lattice sizes already considered and very high quality data for substantially larger lattices. In addition, since different thermodynamic derivatives have peaks at different temperatures, multiple simulations are indeed needed for each lattice size for the optimal extrapolation of effective critical temperatures to the thermodynamic limit for more than one quantity. Such calculations will be quite demanding of computer memory as well as CPU time and are thus not trivial in scope.

In a comprehensive review, Pelissetto and Vicari (2002) have compiled an extensive list of the best numerical results available for the Ising and O(N)

models. The comparison of values for both critical temperatures and critical exponents by Monte Carlo, series expansions, and field theory place the status of both the methods and our knowledge in perspective. Drawing together estimates for critical exponents for different models believed to be in the same universality class and studied by a variety of different methods, one can now generally draw a rather good consensus. For specific, individual models the agreement is less robust and the effects of small, but residual, systematic errors are still problematic. Further discussions of the status of critical exponents, and how they can be determined, can be found in reviews by Zinn-Justin (2001) and Binder and Luijten (2001).

Hasenbusch (2010) has attempted to push the accuracy of the estimates for the critical properties of the Ising model still further and quotes as best estimate for $K_c = 0.221\ 654\ 63(8)$, while the corresponding critical exponent estimates are $\nu = 0.630\ 02(10)$, $\eta = 0.036\ 27(10)$, $\omega = 0.832(6)$.

These numbers fall inside of the crosshatched area of Fig. 7.3, indicating that there is a consensus between different groups. Even if the error bars of Hasenbusch (2010) were still somewhat too optimistic, the above conclusion, drawn a decade earlier – that careful Monte Carlo work (taking corrections to scaling in the finite size scaling analyses into account) yields results on critical properties that are at least as good as those obtained by any other method – is still valid.

Problem 7.1 Consider an Ising square lattice with nearest neighbor ferromagnetic interactions. Carry out a simple, random sampling Monte Carlo simulation of an 8×8 lattice with p.b.c. at $T = \infty$ and construct a histogram of the resultant energy values. Use this histogram to calculate the specific heat at finite temperature and compare your estimates with data from direct importance sampling Monte Carlo simulation. Estimate the location of the 'effective transition temperature' from the histogram calculation. Then, simulate the system at this temperature, construct a new histogram, and recalculate the specific heat. Compare these new results with those obtained by direct importance sampling Monte Carlo simulation. Estimate the temperature at which you would have to simulate the system to get excellent results near the 'effective phase transition' using the histogram method.

7.2.2 The surface-bulk multicritical point: another case study

In this subsection we discuss a problem that illustrates another important principle of Monte Carlo methodologies: to answer a scientific question by simulation of a model system, it is important to think about the most suitable choice of model. For instance, in order to obtain information about critical exponents in the Ising universality class, it is not always the best choice to work with the nearest neighbor Ising model as written in Eqn. (7.18). There can be reasons why other models in the same universality class may do a better job.

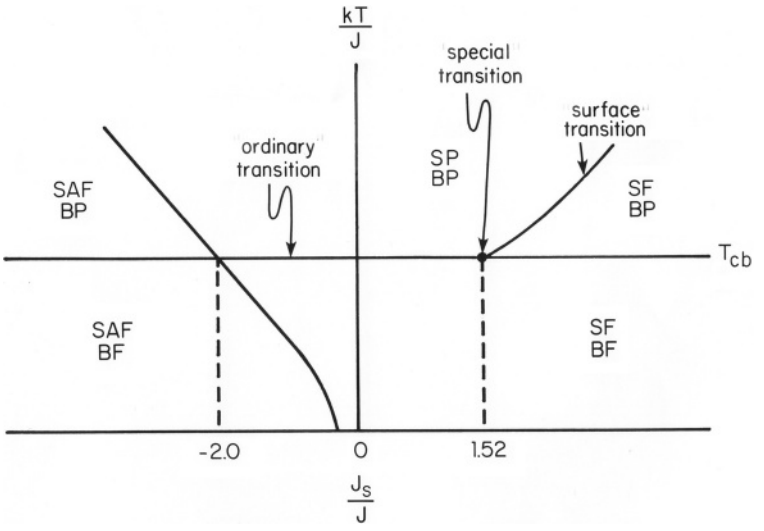

Fig. 7.4 Schematic phase diagram for the semi-infinite Ising model with bulk coupling $\mathcal{J}$ and surface coupling $\mathcal{J}_s$. The bulk transition temperature is T_{cb} and the state of the bulk is denoted BF for a ferromagnet and BP for a paramagnet. The surface phases are labeled SF for a ferromagnet, SP for a paramagnet, and SAF for an antiferromagnet.

Such a situation is encountered when one wishes to extract critical properties associated with free surfaces from finite size scaling studies. We have already mentioned in Section 5.9 that the local magnetization at the surface of an Ising-like system vanishes at the critical temperature T_{cb} of the bulk (remember $k_B T_{cb}/\mathcal{J} = 1/K_c$, in the notation of the previous subsection) with an exponent β_1 different from the exponent β in the (three-dimensional) bulk, $m_1 \propto (1 - T/T_c)^{\beta_1}$. However, as discussed in Section 5.9.1 as well, in systems with free surfaces it is natural to consider an exchange constant $\mathcal{J}_s$ in the surface plane which differs from that in the bulk (see the Hamiltonian written in Eqn. (5.55)). In the absence of any bulk or surface fields, one still expects then an interesting phase diagram, since for $\mathcal{J}_s > \mathcal{J}_{sc}$ the surface of a (semi-infinite) magnet orders before the bulk (Fig. 7.4). Then, m_1 simply shows two-dimensional critical behavior at the critical temperature $T_{cs}(\mathcal{J}_s)$ of this surface transition, $m_1 \propto (1 - T/T_{cs}(\mathcal{J}_s))^{\beta_{2d}}$, with $\beta_{2d} = 1/8$ being the critical exponent of the two-dimensional Ising model. The 'surface-bulk (SB) multicritical point' (also called 'special transition'), where T_{cs} ($\mathcal{J}_s$) merges with the transition of the bulk, $T_{cs}(\mathcal{J}_s) = T_{cb}$ is particularly interesting. Estimation of the critical exponents associated with this multicritical point has been a longstanding challenge (Binder and Hohenberg, 1972, 1974; Diehl and Dietrich, 1981; Binder and Landau, 1984; Landau and Binder, 1990; Ruge *et al.*, 1992; Diehl and Shpot, 1994, 1998; Deng *et al.*, 2005; Hasenbusch, 2011). Methods such as extrapolation of high temperature series expansions (Binder and Hohenberg, 1974) cannot locate the multicritical point with sufficient accuracy, to yield reliable exponent estimates, and the accuracy of renormalization group estimations (Diehl and Dietrich, 1981; Diehl and Shpot, 1994, 1998) is also questionable. Early attempts with Monte Carlo methods (Binder and Landau, 1974; Landau and Binder, 1990) tried to directly estimate exponents via fits of m_1 vs. $1 - T/T_{cb}$ for various values of $\mathcal{J}_s/\mathcal{J}$,

for lattices of rather modest sizes. Of course, with such a straightforward approach problems with locating the multicritical point accurately enough may introduce unknown systematic errors due to unrecognized corrections to scaling.

As discussed in Section 4.2.3 as well as in the previous subsection, the 'method of choice' to study critical properties with Monte Carlo should utilize finite size scaling. For example, studying the dependence of the fourth order cumulant U_4 on $K = \mathcal{J}/k_B T$ and L (see Eqns. (4.12) and (4.14)), one can find the critical point from an analysis of the cumulant intersection. Critical exponents can be extracted from derivatives in the critical region, e.g. for K near K_c we have, repeating Eqn. (4.14),

$$\frac{\partial U_4}{\partial K} = aL^{1/\nu}(1 + bL^{-\omega}), \tag{7.20}$$

where a, b are model-dependent (and hence non-universal) constants, while ν is the correlation length exponent and ω the leading correction to scaling exponent. In the previous subsection we have seen that this method could lead to very accurate estimates of the bulk critical exponents. However, extending this method to surface critical (and multicritical) phenomena encounters a new difficulty: a sub-leading, regular correction of the form L^{-1} (which is absent in systems with periodic boundary conditions) then appears and complicates the analysis. The presence of such an analytic correction can be simply understood from the fact that in a finite $L \times L \times L$ system with two free $L \times L$ surfaces, the geometric distance of these surfaces is $L - 1$ when we have L lattice planes in a lattice direction (remember that the lattice spacing is unity throughout). So here, both L and $L - 1$ enter the description of finite size effects.

Now the innovative step of the methodology used by Hasenbusch (2011) utilizes the universality principle: when the model Hamiltonian contains apart from $\mathcal{J}$ an additional parameter D, amplitude factors such as b will depend on this parameter, while the universal exponents ν, ω are not affected. It turns out that in favorable cases, such as the Blume–Capel model, one can reach a special value $D = D^*$, where $b(D^*) = 0$, so the leading singular correction mentioned above changes its sign. In the Blume–Capel model, spins σ_i can take the three values $\sigma_i = \pm 1, 0$, and the Ising Hamiltonian, Eqn. (7.18), is then complemented by the additional term $-D \sum_i \sigma_i^2$. One can show that the bulk critical exponents of this model are the same as for the Ising model (Hasenbusch, 2010), as expected from the universality principle. Since for this model the critical coupling in the bulk, $K_c(D^*)$, is known with very high precision from a finite size scaling study with periodic boundary conditions in all lattice directions, one just studies quantities such as $U_4(K, K_s = \mathcal{J}_s/k_B T)$ as a function of K_s for fixed $K = K_c(D^*)$ for the system with free surfaces. The leading correction to scaling now is of order $1/L$, and the sub-leading singular correction $L^{-2\omega}$ is clearly much smaller. Under these circumstances, a meaningful finite size scaling analysis becomes possible, but this task would have been much more difficult using the simpler Ising model itself.

Table 7.1 *Results for the surface multicritical exponents y_{h1} and y_{t1}, according to various authors (the methods used are discussed in the main text). For error estimates, see Hasenbusch (2011). Only papers where both exponents were estimated are quoted.*

Authors and year	y_{h1}	y_{t1}
Diehl and Dietrich (1981)	1.65	1.08
Binder and Landau (1984)	1.72	0.89
Landau and Binder (1990)	1.71	0.94
Vendruscolo *et al.* (1992)	1.65	1.17
Ruge *et al.* (1992)	1.62	0.73
Diehl and Shpot (1994)	1.583	0.856
Deng *et al.* (2005)	1.636	0.715
Hasenbusch (2011)	1.646	0.718

In order to actually carry out such a study, state-of-the-art methods are indispensable, alternately sweeping through the lattice with local updates of the spins (using the heat bath algorithm, see Section 5.3.3) and single cluster updates with the Wolff algorithm (see Section 5.1.3). The number of such updates (and also the number of 'measurements' of the relevant observables) ranged from 10^6 to 10^8, for lattice sizes from $L = 8$ to $L = 128$, and single histogram extrapolation was used.

In Section 5.9.7 we emphasized that the quality of pseudo-random numbers is a particularly delicate issue when using the Wolff single cluster algorithm at criticality. For that reason Hasenbusch (2011) used one of the best available pseudorandom number generators, namely the so-called 'Mersenne twister algorithm' (Saito and Matsumoto, 2009). The total computational effort then was the equivalent of 12 years of CPU time in a single core of a Quad-Core AMD Opteron Processor 2378 running at 2.4 GHz.

Table 7.1 compares the critical exponents y_{h1}(note $\beta_1 = \nu(2 - y_{h1})$) and y_{t1} (related to the so-called 'crossover exponent' ϕ by $\phi = \nu y_{t1}$) of this study with previous work obtained by different methods. One can see that the recent, high resolution, finite size scaling studies by Deng *et al.* (2005) and Hasenbusch (2011) give results that are reasonably close to each other, and it is clear that the renormalization group estimates (in particular for y_{t1}) cannot be trusted. For such surface-bulk multicritical problems, high resolution, finite size scaling analyses of Monte Carlo results thus provide the most reliable approach.

7.3 MULTIHISTOGRAM METHOD

If data are taken at more than one value of the varying 'field', the resultant histograms may be combined so as to take advantage of the regions where each provides the best estimate for the density of states. The way in which

this can be done most efficiently was studied by Ferrenberg and Swendsen (1989). Their approach relies on first determining the characteristic relaxation time, τ_j, for the jth simulation and using this to produce a weighting factor $g_j = 1 + 2\tau_j$. The overall probability distribution at coupling K obtained from n independent simulations, each with N_j configurations, is then given by

$$P_K(E) = \frac{\left[\sum_{j=1}^{n} g_j^{-1} H_j(E)\right] e^{KE}}{\sum_{j=1}^{n} N_j g_j^{-1} \, e^{k_j E - f_j}}, \tag{7.21}$$

where H_j(E) is the histogram for the jth simulations and the factors f_j are chosen self-consistently using Eqn. (7.21) and

$$e^{fi} = \sum_{E} P_{K_j}(E). \tag{7.22}$$

Thermodynamic properties are determined, as before, using this probability distribution, but now the results should be valid over a much wider range of temperature than for any single histogram.

7.4 BROAD HISTOGRAM METHOD

The simulation methods which are generally used to produce the histograms for the methods outlined above tend to yield histograms which become increasingly narrower as the lattice size increases; as we saw in Section 7.2. This can lead to such a narrow range over which the reweighting is valid that the applicability of the method is seriously limited. The broad histogram method (de Oliveira *et al.*, 1996) is an attempt to produce histograms which cover a greater range in energy space and which remain useful for quite large systems. The broad histogram Monte Carlo (BHMC) method produces a histogram which spans a wide energy range and differs from other methods in that the Markov process for the method is based upon random walk dynamics. Although the original implementation of this method appears to have been flawed, a modified version has proven to be quite effective for the treatment of Potts glasses (Reuhl, 1997). There has been extensive discussion of whether or not the method, in its various forms, completely obeys detailed balance. Thus, until the broad histogram method is examined more intensively it is premature to say if it will be viewed as an interesting case study in statistical sampling methods or a truly useful research tool.

7.5 TRANSITION MATRIX MONTE CARLO

A method with a similar perspective, but a different implementation, to the broad histogram method is known as 'transition matrix Monte Carlo' (Wang *et al.*, 1999). The method determines a transition matrix, $W(E|E')$, that gives

the time rate of change between states with energies E and E' or a given configuration $\{\sigma\}$ one considers the number $N(\sigma, \Delta E)$ of cases that the energy can change by an amount ΔE for all possible spin-flips. Then for non-zero ΔE,

$$W(E + \Delta E|E) = w(\Delta E)\langle N(\sigma, \Delta E)\rangle_{\mathrm{E}}, \tag{7.23}$$

where the average is over all configurations having energy E, and $w(\Delta E)$ is some spin-flip rate, e.g. the Glauber rate, that is used in a simulation to determine the elements of the transition matrix. Note that the kinetics of the transition matrix method differs from that of the 'traditional' single spin-flip approaches, but the method obeys detailed balance which, in turn, places strong constraints on the matrix elements. Once the transition matrix is determined it can be used to estimate canonical probabilities.

7.6 MULTICANONICAL SAMPLING

7.6.1 The multicanonical approach and its relationship to canonical sampling

In some cases the probability distribution for the states of the system will contain multiple maxima which are widely spaced in configuration space. (Examples include systems near first order phase transitions and spin glasses.) Standard methods may 'flow' towards one of the maxima where they may be easily 'trapped'. Transitions between maxima may occur but, as long as they are infrequent, both the relative weights of the multiple maxima as well as the probability distribution between maxima will be ill determined. One effective approach to such circumstances is to modify the traditional single spin-flip probability to enhance the probability that those 'unlikely' states between the maxima occur. This is not always easy to do and often multiple 'trial runs' must first be made in order to determine what is the best probability to use.

This method reformulates the problem in terms of an effective Hamiltonian:

$$\mathcal{H}_{\mathrm{eff}}(\sigma) = H_{\mathrm{eff}}(\beta\mathcal{H}(\sigma)). \tag{7.24}$$

The probability distribution for the energy can then be written as

$$P(E) = \frac{\exp(S(E) - \mathcal{H}_{\mathrm{eff}})}{\sum_E \exp(S(E) - \mathcal{H}_{\mathrm{eff}})}. \tag{7.25}$$

In the multicanonical algorithm (Berg and Neuhaus, 1991, 1992) the desired form of the probability of states with energy E is determined self-consistently by performing a simulation and using the resultant distribution as a probability estimate for a second simulation, etc. The 'final' probability found is shown in Fig. 7.5, where we show the probability in the canonical ensemble for comparison. Thus, a substantial fraction of the computer resources needed to solve a problem with the multicanonical ensemble may be consumed in the effort to find an optimum probability distribution. The resultant estimate

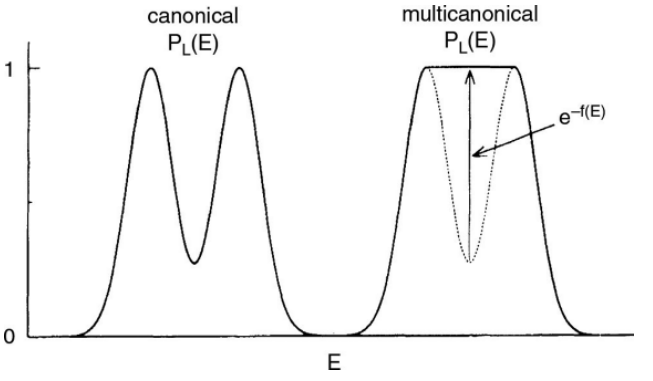

Fig. 7.5 Probability distribution for canonical Monte Carlo sampling for a model with multiple minima compared to that for multicanonical Monte Carlo.

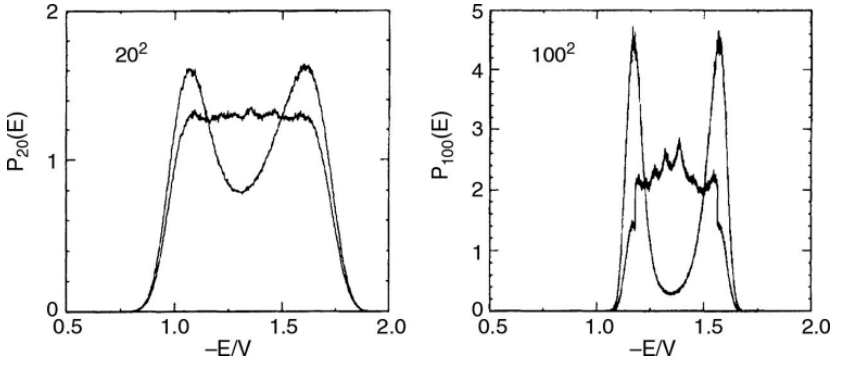

Fig. 7.6 Multicanonical energy distribution $P'_L(E)$ together with the reweighted canonical distribution $P_L(E)$. Both distributions are normalized to unit area. After Janke (1992).

of a thermodynamic average is given by

$$\langle A \rangle_\beta = \frac{\langle A \exp(\mathcal{H}_{\text{eff}} - \mathcal{H}) \rangle}{\langle \exp(\mathcal{H}_{\text{eff}} - \mathcal{H}) \rangle}, \tag{7.26}$$

and it is more likely to give correct answers in a situation where the energy landscape is quite complicated than most canonical ensemble methods.

A practical approach to the determination of the effective Hamiltonian is to first determine the probability distribution of states under conditions for which it is easy to measure using a standard Monte Carlo method. Then, use this distribution as an estimate for another run which is made closer to the region of real interest. This process continues all the way to the 'unknown' region where standard sampling methods fail.

As an example of the applicability of the multicanonical algorithm, in Fig. 7.6 we show the results for a $q = 7$ Potts model, a system which has a fairly strong first order transition. The simulations were performed on $L \times L$ square lattices with periodic boundary conditions. For $L = 20$ the multicanonical distribution is quite flat even though the reweighted, canonical distribution shows two clear peaks. For $L = 100$, it is clearly difficult to find a smooth multicanonical probability, but the resultant canonical distribution shows two

smooth and very pronounced peaks. Obtaining the relative heights of these two maxima would have been quite difficult using canonical sampling.

7.6.2 Near first order transitions

Having made the above qualitative remarks and given the example shown in Fig. 7.6, intended to whet the appetite of the reader to learn more about multicanonical sampling, we now proceed to examine the situation near a standard first order transition in greater detail. The systems which we have in mind are the q-state Potts models, which have thermally driven first order transitions in $d = 2$ for $q > 4$, in $d = 3$ for $q \geq 3$, and – even simpler – the transition of the Ising ferromagnet as a function of magnetic field H for $T < T_c$. Remember (see, e.g. Sections 2.1.2.4, 2.3.2, 4.2.3.3, 4.2.5.4) that at $H = 0$ the order parameter (i.e. the magnetization) jumps from a positive value (M_+) to a negative value ($M_- = -M_+$, cf. Fig. 2.10), and this is accompanied by a dramatic (exponential!) increase of the relaxation time τ_e with lattice size for transitions between states of opposite magnetization in the framework of a simulation with the Metropolis algorithm. Actually this 'ergodic time' τ_e was already roughly estimated in Eqn. (4.65). In the literature (e.g. Berg, 1997) this exponential variation of τ_e with L is sometimes called 'supercritical slowing down'. By the multicanonical method, or its variants, one is able to reduce the correlation time τ to a power law of size dependence, $\tau \propto L^p$. While p is rather large, namely $2d \leq p \leq 5d/2$ where d is the dimension of the lattice (Berg, 1997), the method is clearly useful for large L: while in Fig. 7.6 the minimum and maximum values of $P_L(E)$ differ only by about a factor of 10, there are other examples where maximum and minimum of the distribution differ by astronomically large factors, e.g. in the study of symmetrical polymer mixtures (Müller *et al.*, 1995) the difference was up to a factor of 10^{45} at temperatures far below criticality. Variations of the multicanonical method have also proven to be effective including the 'multimagnetical method' (Berg *et al.*, 1993), where a flat distribution $P'_L(M)$ of the magnetization M is constructed in between M_- and M_+ in analogy to the flat distribution $P'_L(E)$ shown in Fig. 7.5, and the 'multibondic algorithm' (Janke and Kappler, 1995), where a combination with cluster algorithms is worked out.

We now consider how to make the step from the canonical distribution $P_L(E)$, in Fig. 7.5, to the multicanonical one, $P'_L(E)$, which has the property $P'_L(E) = \text{const.}$ for $E_{\min} < E < E_{\max}$, with $\varepsilon_{\min} = E_{\min}/L^d < \varepsilon_{\max} = E_{\max}/L^d$ being constants as $L \to \infty$, by a first-principles approach (following Berg, 1997). This task is achieved by reweighting the canonical distribution $P_L(E)$ with a weight factor $W(E)$ which is related to the spectral density of states $n(E)$ or the (microcanonical) entropy $S(E)$,

$$W(E) = 1/n(E) = \exp[-S(E)] \equiv \exp[-\beta(E)E + \alpha(E)]. \qquad (7.27)$$

In the last step we have introduced the inverse temperature $1/T(E) = \beta(E) = \partial S(E)/\partial E$ and thus the problem is to construct the, as yet unknown, function $\alpha(E)$ (at least up to an additive constant). This problem in principle can be

solved recursively. For a model where the energy spectrum is discrete (such as Ising, Potts models, etc.), there is a minimum spacing between energy levels, which we denote as δE here. Then the discrete analog of the above partial derivative $\beta(E) = \partial S(E)/\partial E$ becomes

$$\beta(E) = [S(E + \delta E) - S(E)]/\delta E, \tag{7.28}$$

and using the identity (from Eqn. (7.27)) $S(E) = \beta(E)\, E - \alpha(E)$ we can write

$$\begin{aligned} S(E) - S(E - \delta E) = \beta(E)E - \beta(E - \delta E)(E - \delta E) \\ - [\alpha(E) - \alpha(E - \delta E)]\,. \end{aligned} \tag{7.29}$$

Eliminating now the entropy difference on the left-hand side of Eqn. (7.29) with the help of Eqn. (7.28) we find the recursion

$$\alpha(E - \delta E) = \alpha(E) + [\beta(E - \delta E) - \beta(E)]E, \tag{7.30}$$

where $\alpha(E_{\max} = 0)$ is a convenient choice of the additive constant.

In order to use Eqn. (7.29), we would have to do a very accurate set of microcanonical runs in order to sample the relation $\beta = \beta(E)$ from $E_{\max}$ to $E_{\min}$, and this requires of the order $L^{d/2}$ different states (which then can be combined into one smooth function by multihistogram methods, see above). The multicanonical sampling of the flat distribution $P'_L(E)$ itself (obtained by reweighting with $W(E)$ in Eqn. (7.26), once the weights are estimated) is then a random walk in the energy space, and hence implies a relaxation time $\tau \propto L^{2d}$ since the 'distance' the random walker has to travel scales as $E_{\max} - E_{\min} \propto L^d$. Actually, in practice the recursion in Eqn. (7.30) may be avoided for a large system, because good enough weights $\alpha(E)$ can often be obtained from a finite size scaling-type extrapolation from results for small systems. Still, the problem remains that τ scales as L^{2d}, a rather large power of L. An alternative to the procedure outlined above involves using the inverse of the histogram obtained between $E_{\max}$ and $E_{\min}$ at a higher temperature as an estimate for the weighting function. A short multicanonical run is made using this estimate and then the resultant distribution is used to obtain an improved weight factor to be used for longer runs (Janke, 1997).

While the pioneering studies of finite size scaling at first order transitions described in Section 4.2.3.3 used the Metropolis algorithm, and thus clearly suffered from the problem of 'supercritical slowing down', rather accurate studies of Potts models with the multicanonical algorithm are now available (Berg, 1997). Various first order transitions in lattice gauge theory have also been studied successfully with this method (see Berg (1997) and Chapter 11 of the present book).

7.6.3 Groundstates in complicated energy landscapes

We have encountered complicated energy landscapes in systems with randomly quenched competing interactions, such as spin glasses (Section 5.4.4),

and related problems with conflicting constraints (e.g. the 'traveling salesman problem', Section 5.4.4). It is also possible to treat such problems with a variant of multicanonical methods, only the recursion is done slightly differently by starting high up in the disordered phase, where reliable canonical simulations can be performed. In the extreme case $E_{\max}$ is chosen such that the corresponding temperature is infinite, $\beta^0(E_{\max}) = 0$ and then a recursion is defined as (Berg, 1996, 1997)

$$\beta^{n+1}(E) = (\delta E)^{-1} \ln[H_0^k(E + \delta E)/H_\beta^n(E)], \tag{7.31}$$

where $H_0^k(E)$ is the (unnormalized) histogram obtained from a simulation at $\beta^k(E)$, while H_β^n contains combined information from all the runs with $\beta^0(E), \ldots, \beta^n(E)$:

$$H_\beta^k(E) = \sum_{k=0}^{n} g_k(E) H_\beta^k(E), \tag{7.32}$$

and the factors $g_k(E)$ weigh the runs suitably (see Berg (1996, 1997) for details). With these techniques, it has become possible to estimate rather reliably both groundstate energy and entropy for $\pm\mathcal{J}$ nearest neighbor Edwards–Anderson spin glasses in both $d = 2$ and $d = 3$ dimensions. However, the slowing down encountered is very bad ($\tau \propto L^{4d}$ or even worse) and thus the approach has not been able to finally clarify the controversial aspects about the spin glass transition and the nature of the spin glass order (two-fold degenerate only or a phase space with many 'valleys'?) so far.

At this point we draw attention to a related method, namely the method of expanded ensembles (Lyubartsev *et al.*, 1992), where one enlarges the configuration space by introducing new dynamical variables such as the inverse temperature (this method then is also called 'simulated tempering'; see Marinari and Parisi (1992)). A discrete set of weight factors is introduced

$$w_k = \exp(-\beta_k E + \alpha_k), \quad k = 1, \ldots, n, \quad \beta_1 < \beta_2 < \cdots \beta_{n-1} < \beta_n. \tag{7.33}$$

The transitions $(\beta_k, \alpha_k) \to (\beta_{k-1}, \alpha_{k-1})$ or $(\beta_{k+1}, \alpha_{k+1})$ are now added to the usual $E \to E'$ transitions. Particularly attractive is the feature that this method can be efficiently parallelized on n processors ('parallel tempering', Hukusima and Nemoto (1996)).

Just as the multicanonical averaging can estimate the groundstate energy of spin glass models, it also can find the minimum of cost functions in optimization problems. Lee and Choi (1994) have studied the traveling salesman problem with up to $N = 10\,000$ cities with this method.

7.6.4 Interface free energy estimation

Returning to the magnetization distribution $P_L(M)$ of the Ising model for $T < T_c$, we remember (as already discussed in Section 4.2.5.4) that the minimum

of $P_L(M)$ which occurs for $M \approx 0$ is realized for a domain configuration, where two domain walls (of area L^{d-1} each) run parallel to each other through the (hyper-cubic) simulation box, such that one half of the volume L^d is in a domain with magnetization M_+, and the other half of the volume forms the domain with magnetization $M_- = -M_+$. Thus, the free energy cost of this configuration (relative to a state with uniform magnetization M_+ or M_-, respectively) is estimated as $2\sigma L^{d-1}$, σ being the interfacial tension. Hence one predicts (Binder, 1982) that $P_L(M=0)/P_L(M_+) = \exp(-2\beta\sigma L^{d-1})$. Since this ratio, however, is nothing but the weight $W(M)$ needed to convert $P_L(M)$ to the flat distribution $P'_L(M)$, it follows that we can estimate σ if we know this weight:

$$\sigma = -\frac{1}{2\beta L^{d-1}} \lim[P_L(M=0)/P_L(M_+)]. \tag{7.34}$$

While the first application of this idea for the Ising model (Binder, 1982) using the Metropolis algorithm failed to obtain accurate results, combination with multicanonical methods did produce very good accuracy (Berg *et al.*, 1993). Meanwhile these techniques have been extended to estimate interfacial tensions between the ordered and disordered phases of Potts models (Berg, 1997), coexisting vapor and liquid phases of various fluids such as CO_2, benzene, etc. (Mognetti *et al.*, 2008), coexisting phases in polymer mixtures (Müller *et al.*, 1995), and various models of lattice gauge theory (see Chapter 11).

At this point, we emphasize that the reweighting techniques described in this section are still a rather recent development and form an active area of research; thus we have not attempted to describe the algorithms in full detail but rather give the flavor of the various approaches.

Problem 7.2 Use the multicanonical sampling method to determine the energy histogram for a 16×16 Ising square lattice at $k_B T/J = 2.0$. From these data determine the canonical ensemble distribution and compare with the distribution obtained from Metropolis Monte Carlo simulation.

7.7 A CASE STUDY: THE CASIMIR EFFECT IN CRITICAL SYSTEMS

Before ending this chapter, we wish to briefly review a Monte Carlo study which could not have been successful without use of the combination of advanced sampling techniques discussed in Chapter 5 together with the reweighting methods presented in this chapter. If a critical system is confined between two walls, critical fluctuations of the order parameter generate effective long range interactions which are reminiscent of those due to zero point fluctuations of the electromagnetic spectrum for a system of two closely spaced magnetic plates. This phenomenon, known as the Casimir effect, can be described in terms of

universal amplitudes which determine the strength of the contribution to the effective interface potential due to a term proportional to $\Delta l^{-(d-1)}$ where l is the thickness of the film and Δ is known as the Casimir amplitude. The direct determination of the Casimir amplitudes is quite difficult since it demands the very careful measurement of the small free energy difference between two systems with different boundary conditions. A careful study of the Casimir amplitudes of two-dimensional and three-dimensional Potts models with different boundary conditions was performed by Krech and Landau (1996). The system was divided into two pieces, e.g. in two dimensions an $L \times M$ system was divided into two strips of width $L/2$ coupled through a seam Hamiltonian so that

$$\mathcal{H}_\lambda = \mathcal{H} + \lambda \mathcal{H}_{\text{seam}}. \tag{7.35}$$

They used a hybrid Monte Carlo sampling algorithm which combined Metropolis and Wolff steps and umbrella sampling to simulate $L \times M$ square lattices. The difference in free energy with and without the seam gave the combination of different Casimir amplitudes as $L, M \to \infty$ but with fixed aspect ratios. In Fig. 7.7 the histograms produced by simulations for different values of λ show just how little overlap there is between curves unless their λ values are quite close together. Even with the improved sampling algorithm, extensive sampling was needed and 7.2×10^5 hybrid steps were used to produce each of the histograms shown in Fig. 7.7. Note that the spacing of the histograms changes with λ and it is important to choose the values of λ which produce adequate overlap of the histograms. On the right in this figure the results for three different Potts models are compared with the exact answers. Other Casimir amplitudes were measured, including some for which the answer is not known.

7.8 WANG–LANDAU SAMPLING

7.8.1 Basic algorithm

A different approach to Monte Carlo sampling was recently proposed (Wang and Landau, 2001), and it has already been shown not only to be quite powerful but also to have quite wide applicability. The method is related in spirit to the multicanonical Monte Carlo and umbrella sampling techniques and their variations ('broad histogram Monte Carlo', 'flat histogram Monte Carlo', etc.) that were discussed earlier in this chapter. It also has the merit of greater simplicity and, unlike other methods, it is rather straightforward to implement and is, hence, potentially much more useful. This new Monte Carlo method, the 'random walk in energy space with a flat histogram', has become broadly known as 'Wang–Landau sampling'. In this approach we recognize that the

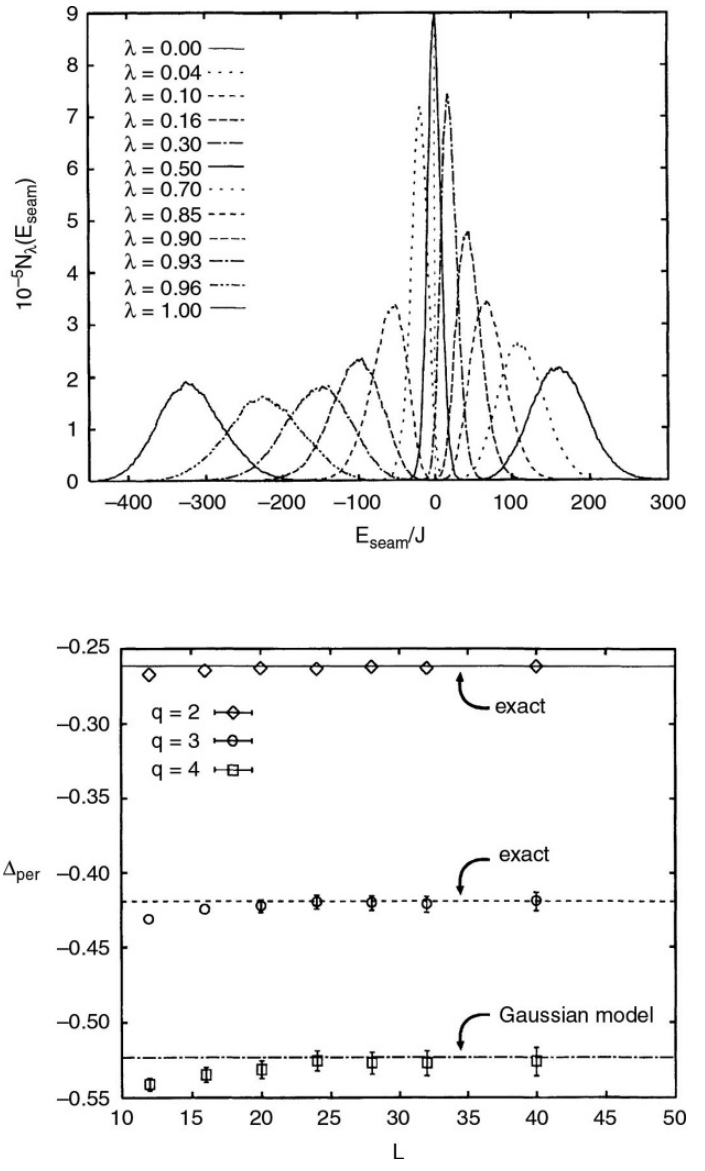

Fig. 7.7 (top) Histograms for the $q = 4$, 320×40 Potts model with periodic boundary conditions; (bottom) Casimir amplitude Δ_{per} for q-state Potts models with fixed aspect ratio of 1/8. After Krech and Landau (1996).

classical partition function can either be written as a sum over all states or over all energies, i.e. we can rewrite Eqn. (2.1) in a different, but equivalent, form

$$Z = \sum_i e^{-E_i/k_B T} \equiv \sum_E g(E) e^{-E/k_B T} \tag{7.36}$$

where $g(E)$ is the density of states. Since $g(E)$ is independent of temperature, it can be used to find all properties of the system at all temperatures. Of course, the density of states may be expressed as a function of multiple variables, e.g. $g(E, M)$ where M is the magnetization, but for pedagogical purposes we

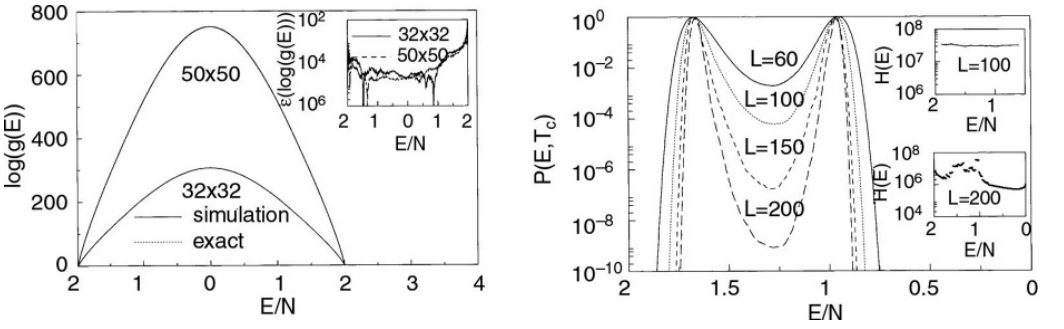

Fig. 7.8 Typical results from 'Wang–Landau sampling'. (Left) Density of states for $L \times L$ Ising square lattices. The inset shows the relative errors. (Right) Canonical probability for $L \times L$ $q = 10$ Potts models. Final histograms are in the inset. Note that for the $q = 10$ Potts model with $L = 200$ the energy range has been divided into multiple intervals and parallel walks have taken place over each interval. After Wang and Landau (2001).

shall restrict ourselves to the one-dimensional case in the following discussion. Wang–Landau sampling is a flexible, powerful, iterative algorithm to estimate $g(E)$ directly instead of trying to extract it from the probability distribution produced by 'standard' Monte Carlo simulations. We begin with some simple 'guess' for the density of states, e.g. $g(E) = 1$, and improve it in the following way. Spins are flipped according to the probability

$$p(E_1 \rightarrow E_2) = \min\left(\frac{g(E_1)}{g(E_2)}, 1\right) \tag{7.37}$$

where E_1 is the energy before flipping and E_2 is the energy that would result if the spin were flipped. Following each spin-flip trial the density of states is updated,

$$g(E) \rightarrow g(E) f_i \tag{7.38}$$

where E is the energy of the resultant state (i.e. whether the spin is flipped or not) and f_i is a 'modification factor' that is initially greater than 1, e.g. $f \sim e^1$. A histogram of energies visited is maintained, and when it is 'flat' the process is interrupted, f is reduced, e.g. $f_{i+1} = \sqrt{f_i}$, all histogram entries are reset to zero, and the random walk continues using the existing $g(E)$ as the starting point for further improvement. We emphasize here that the histogram of energies visited does not have to be perfectly flat, and it typically suffices if the minimum entry is ~80% of the mean value. In the early stages 'detailed balance' is not satisfied, but as $f_i \rightarrow 1$ it is recovered to better than statistical precision. The extraordinary agreement with exact results for the Ising square lattice is shown in Fig. 7.8. The application to systems as large as $L = 256$, for which $g(E)$ is not known, yielded excellent agreement with exact values for thermodynamic properties. At this juncture we note that the method allows the straightforward determination of entropy and free energy, quantities that can only be obtained indirectly from standard, canonical ensemble Monte Carlo methods.

Wang–Landau Monte Carlo scheme

(1) Set $g(E) = 1$; choose a modification factor (e.g. $f_0 = e^1$).
(2) Choose an initial state.
(3) Choose a site i.
(4) Calculate the ratio of the density of states

$$\eta = \frac{g(E_1)}{g(E_2)}$$

which results if the spin at site i is overturned.
(5) Generate a random number r such that $0 < r < 1$.
(6) If $r < \eta$, flip the spin.
(7) Set $g(E_i) \rightarrow g(E_i) * f$.
(8) If the histogram is not 'flat', go to the next site and go to (4).
(9) If the histogram is 'flat', decrease f, e.g. $f_{i+1} = f_i^{1/2}$.
(10) Repeat steps (3)–(9) until $f = f_{\min} \sim \exp(10^{-8})$.
(11) Calculate properties using final density of states $g(E)$.

In Fig. 7.8 we compare the values of $g(E)$ obtained by this iterative method with the exact values found for finite Ising square lattices. The agreement is obviously excellent. The canonical probability that was determined in this way for the two-dimensional 10-state Potts model, which is known to have a strong first order phase transition, has two peaks at T_c (corresponding to disordered and ordered states) with very low probability in between. Standard Monte Carlo methods 'tunnel' between peaks poorly and the relative magnitudes of the peaks cannot be estimated. In Fig. 7.8 we see that up to *nine orders of magnitude* difference in probability was measurable with this method. For the largest values of L the energy range was broken up into multiple sub-intervals and independent random walks were performed over each energy interval. The different pieces of $g(E)$ were then joined together using the condition that they needed to match at the boundaries of the energy ranges.

An even more stringent test of the ability of Wang–Landau sampling to probe the complex energy landscape was the application to the three-dimensional Edwards–Anderson spin glass model. Here the sampling was carried out as a two-dimensional random walk in energy-order parameter space where the order parameter q was the spin glass order parameter and not the uniform magnetization. Using the resultant $g(E, q)$ and reweighting with the appropriate Boltzmann factor, Wang and Landau (2001) showed that up to *30 orders of magnitude* in the canonical probability was accessible with this method (see Fig. 7.9). This 'feasibility test' showed that the method was also effective for a model with a quite rough energy landscape. Of course, for the study of spin glasses it is necessary to use a large number of bond configurations (typically 10^3), and the production of such averaged data of high quality for a wide range of temperature (and thus energy) and linear dimensions is still beyond reach.

Numerous applications of this method have already resulted, and it is impossible to list all of them. We do wish to draw the reader's attention to

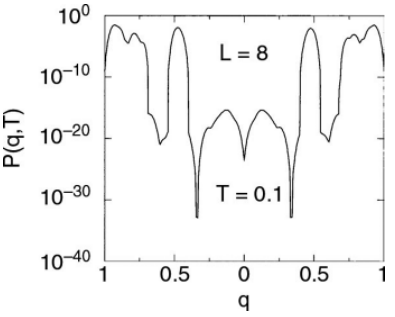

Fig. 7.9 Canonical probability for the EA spin glass model at low temperature. This result is for a single distribution of bonds. After Wang and Landau (2001).

improved sampling algorithms (Schulz *et al.*, 2002, 2003; Yamaguchi and Kawashima, 2002), and applications of the method to models with continuous symmetries. Models of the latter type include proteins (e.g. Rathore *et al.*, 2003); polymer films (Jain and de Pablo, 2002); and continuum (fluid) models (e.g. Shell *et al.*, 2002; Jain and de Pablo, 2003; Yan and de Pablo, 2003). By a suitable reformulation of the problem Troyer *et al.* (2003) also showed how Wang–Landau sampling could be used for quantum problems, and even the Kondo problem has been examined (Koller *et al.*, 2003). Some understanding of the convergence and performance limitations of the method have already been provided (Dayal *et al.*, 2004; Zhou and Bhatt, 2004). The wide range of types of problems for which Wang–Landau sampling has already proven to be beneficial is extremely promising.

7.8.2 Applications to models with continuous variables

Many of the models that we have already discussed have continuous variables rather than discrete ones. In principle there are then an infinite number of energies to be considered. The simplest approach is to simply 'bin' the energy into small regions of energy with a small width, but the use of a kernel function update scheme improves the resultant density of states. This is not enough to handle the singularity that occurs in $g(E)$ as the groundstate is approached, so the method of 'frontier sampling' was developed to overcome this difficulty (Zhou *et al.*, 2006). The simulation is 'pushed' into the unexplored, low energy region through the introduction of a global update. This approach has proven to be effective for a variety of models, including Heisenberg magnets and proteins (see Chapter 14). Some applications of the Wang–Landau algorithm to off-lattice models have been reviewed by Müller and de Pablo (2006).

7.8.3 A simple example of two-dimensional Wang–Landau sampling

A further advantage of Wang–Landau sampling is that it may be easily extended to a random walk in a multidimensional parameter space. For a simple Ising model it might be advantageous to perform a random walk in both energy and magnetization and thus extract all of the properties as a function of both temperature and magnetic field from a single simulation. This approach is

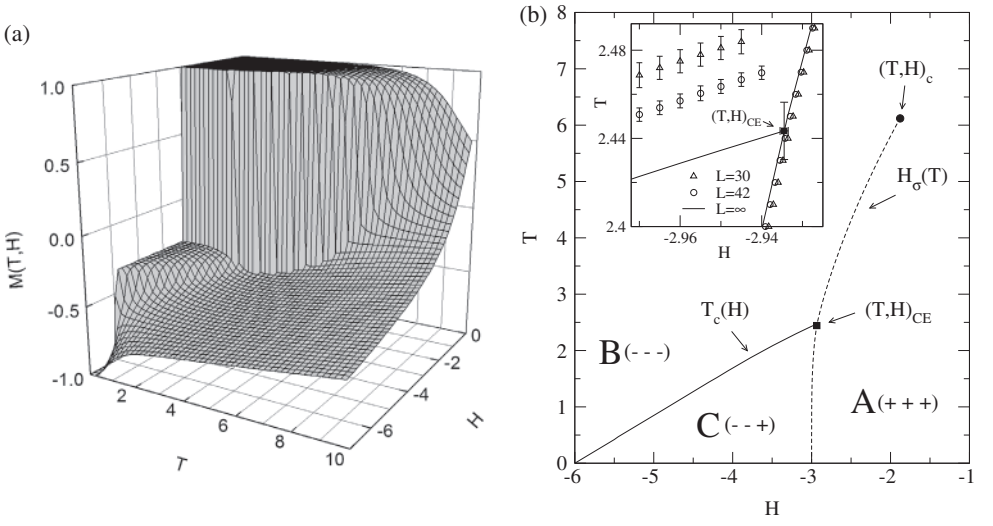

Fig. 7.10 (a) Magnetization for the triangular Ising model with nearest and next nearest neighbor interactions computed from the two-dimensional density of states; (b) resultant phase diagram in T–H space showing the critical endpoint $(T, H)_{CE}$. From Tsai *et al.* (2007).

particularly useful when, e.g., there is no special symmetry and a critical point of interest must be searched for in a space of more than one variable. As an example, we consider a recent study on the critical endpoint behavior in an asymmetric Ising ferrimagnet (Tsai *et al.*, 2007). The model is quite simple; Ising spins are placed on a triangular lattice and interact with nearest neighbors via both two-spin and three-spin coupling:

$$\mathcal{H} = -\mathcal{J}_{nn} \sum_{i,k} \sigma_i \sigma_k - \mathcal{J}_3 \sum_{i,j,k} \sigma_i \sigma_j \sigma_k - H \sum_i \sigma_i . \tag{7.39}$$

Although it has been known for two decades that the phase diagram contained a critical endpoint, it was impossible using existing technologies to study the behavior in the vicinity of the critical endpoint with high resolution.

In Fig. 7.10a the magnetization of this model in the canonical ensemble computed using the two-dimensional density of states $g(E, M)$ from a *single simulation* is depicted as a function of both temperature and magnetic field. Figure 7.10b shows the resultant phase diagram that is extracted, showing the location of the critical endpoint.

7.8.4 Microcanonical entropy inflection points

Wang–Landau sampling provides us with the ability to determine the entropy directly, and with high precision, using the density of states instead of via thermodynamic integration. For some systems, such as proteins, the finite size of the system is an intrinsic property of the model and finite size scaling cannot be applied. Recently, Schnabel *et al.* (2011) showed how the behavior of the energetic derivative of the microcanonical entropy, i.e. the inverse

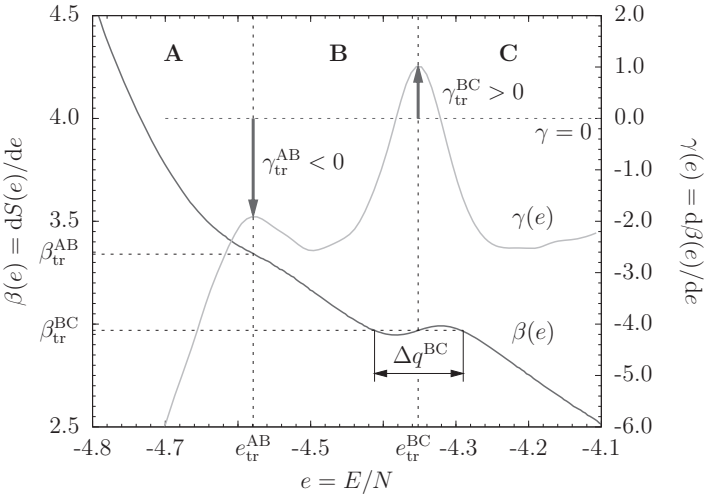

Fig. 7.11 Inverse temperature and its derivative $\gamma(E)$ vs. energy for an elastic polymer. The maxima in $\gamma(E)$ denote transitions; the transition between A and B is the analog of a second order transition because $\gamma(E) < 0$ and between B and C is the analog of a first order transition, i.e. $\gamma(E) > 0$. After Schnabel *et al.* (2011).

microcanonical temperature, would allow a systematic classification for the analogs of phase transitions in finite systems. Defining the microcanonical temperature by

$$\beta(E) = T^{-1}(E) = (dS/dE)_{N,V}, \tag{7.40}$$

one can further define the derivative

$$\gamma(E) = d\beta(E)/dE = d^2S/dE^2. \tag{7.41}$$

The behavior of inflection points in the microcanonical temperature then not only indicates the occurrence of a 'transition' but also indicates if it is first order or second order equivalent. Such an analysis demands very precise knowledge of the microcanonical entropy, but, as shown in Fig. 7.11, the results can be quite convincing.

When talking about 'transitions' in finite systems one must keep in mind, of course, that for finite systems the different ensembles of statistical thermodynamics are not equivalent. (Legendre transformations only apply in the thermodynamic limit.) Thus, if a polymer is in solution, the physical situation normally corresponds to a canonical rather than a microcanonical ensemble. In that case both 'transitions' in Fig. 7.11 would show rounded peaks in the specific heart as a function of temperature.

7.8.5 Back to numerical integration

In Section 3.2 we discussed a few methods for using Monte Carlo for numerical integration. Such techniques are known to have advantages over traditional algorithms for evaluating higher dimensional integrals; however, applications of conventional Monte Carlo integration methods are also limited. For instance, convergence may be slow and, even with a large amount of sampling to reduce the statistical error, convergence is not always assured.

The importance sampling Monte Carlo method for numerical integration (considering one-dimensional integration for pedagogical purposes) introduces a probability weighting function $p(x)$ which mimics the integrand $y = f(x)$ and generates points according to the flattened ratio $f(x)/p(x)$ instead of the original integrand. Limitations arise because $p(x)$ has to be positive and normalized to unity in the integration domain and this implies knowledge of the behavior of $f(x)$. Such information is not always available for a complicated function; furthermore, importance sampling may not even converge to the correct values if a 'poor' weighting function is chosen.

As an application of their self-adaptive range Wang–Landau algorithm, Tröster and Dellago (2005) adapted Wang–Landau sampling to the problem of numerical integration. They first expressed the integrand $f(x)$ in terms of a 'Boltzmann factor' $e^{-\phi}(x)$ with $\phi(x) = \ln f(x))$ with $k_B T = 1$. The remaining problem was treated with simple Wang–Landau sampling; however, the formulation is restricted to positive integrands $f(x) > 0$ because of the logarithm. A different formulation, however, allows Wang–Landau sampling to be applied to numerical integration without this limitation (Li *et al.*, 2007). A means by which a definite integral $\int_a^b f(x)dx$ may then be evaluated is to determine the proportion of integration domain that lies within a certain interval $[y, y + dy]$. A distribution depending on y, namely $g(y)$, can be generated measuring this fraction, and this quantity is analogous to the density of states $g(E)$ for a model in statistical physics. Provided that the lower bound $y_{\min}$ and the upper bound $y_{\max}$ of the integrand are known, the integral can then be approximated by

$$I = -\int_a^b f(x)dx = \sum_{y_{\min}}^{y_{\max}} g(y) \cdot y. \tag{7.42}$$

Since the algorithm provides only a relative distribution function $g(y)$, the answer has to be normalized appropriately. Of course, the lower and upper bounds, $y_{\min}$ and $y_{\max}$, respectively, of the integrand $f(x)$, as well as y values that cannot be reached within the integration domain, must first be determined. The valid range in y space can be found from an initial 'domain sampling run' (Tröster and Dellago, 2005). The technique for one-dimensional Wang–Landau integration can be easily generalized to higher dimensional integrals, and Li *et al.* (2007) showed that the method works quantitatively for sample one-dimensional and two-dimensional integrals with integrands that are far from 'flat'. In addition, the application of the approach to a 'real' physics research problem was illustrated by the evaluation of integrals arising in perturbation theory of quantum many-body systems.

7.8.6 Replica exchange Wang–Landau sampling

We have seen in previous sub-sections that Wang–Landau sampling is a simple, broadly applicable Monte Carlo procedure with only a minimal set of

adjustable parameters. It has been applied successfully to quite diverse problems and various improvements have been proposed to the method, e.g. by optimizing the 'modification factor and flatness criterion' scheme or by implementing novel Monte Carlo trial moves. (see Vogel *et al.* (2013) for more detail). Ultimately, however, parallelization is the only means to systematically improve the performance for ever larger problems on increasingly complex, massively parallel machines. An early attempt at parallelization subdivided the total energy range into smaller windows, each sampled by an independent Wang–Landau random walker. The total simulation time was limited by the convergence of the slowest walker but could be tuned by unequal distribution of energy space. However, an optimal load balancing was impossible due to the a priori unknown irregularities in the free energy landscape. Furthermore, as energy intervals are reduced the sampling may become non-ergodic. Alternatively, multiple random walkers could work simultaneously on the same density of states and histogram; however, such a massively parallel implementation (Yin and Landau, 2012) revealed that correlations among the walkers can systematically underestimate $g(E)$ in 'difficult to access' energy regions. The addition of an *ad hoc* bias to the modification factor solved the problem in this case; but, overall, such solutions are undesirable.

A novel, new approach to parallelization is a quite generic scheme that combines the advantageous dynamics of Wang–Landau sampling with the idea of replica-exchange Monte Carlo simulations (see Section 5.4.2). The total energy range is split up into smaller windows but with large overlap between adjacent sub-windows. Each energy window is then sampled by multiple, independent Wang–Landau walkers. The key improvement in this algorithm is that configurational, or 'replica', exchanges are allowed between overlapping energy windows during the course of the simulation. This allows each replica to travel back and forth through the entire energy space but does not bias the overall Wang–Landau procedure and is valid for any update rule. Since it does not impose any principal limitation to the number of Wang–Landau replicas, the framework may scale up to many hundreds of thousands of CPUs.

To be more specific, in this parallel Wang–Landau scheme the global energy range is split into h smaller intervals (windows), each of which contains m random walkers. Consecutive windows must overlap each other to allow for configurational exchange (examples are shown in Fig. 7.12). The magnitude of the overlap should be chosen to strike a balance between fast convergence of $g(E)$ and a reasonable exchange acceptance rate. (A large overlap of $\sim$75% worked well, but excellent results can be obtained with other choices.) Within an energy window, each random walker performs standard Wang–Landau sampling. After a certain number of Monte Carlo steps, a replica exchange is attempted between two random walkers, i and j, where walker i chooses swap partner j from a neighboring window at random. Let X and Y be the configurations that the random walkers i and j are carrying before the exchange, and $E(X)$ and $E(Y)$ be their energies, respectively. To ensure fulfillment of the detailed balance condition the acceptance probability P_{acc} for

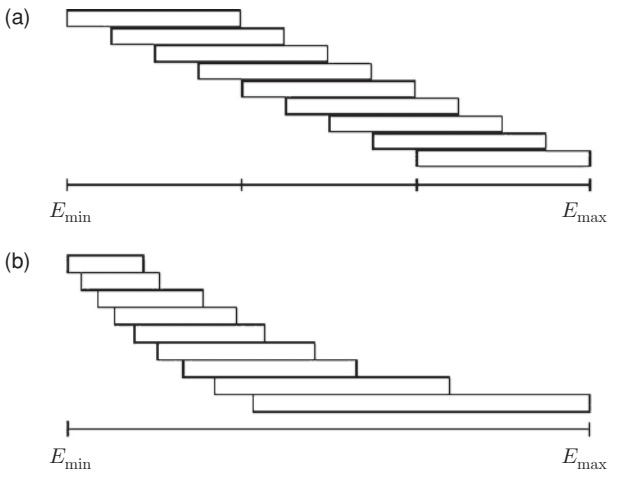

Fig. 7.12 Schematic view of possible subdivisions of the total energy range into overlapping windows for replica exchange Wang–Landau sampling. (a) Partition of the global energy range into nine equal windows with 75% overlap; (b) run-time balanced partition with 75% overlap to the higher energy window. From Vogel *et al.* (2013).

the exchange of configurations X and Y between walkers i and j is

$$P_{\text{acc}} = \min\left[1, \frac{g_i(E(X))}{g_i(E(Y))}\frac{g_j(E(X))}{g_j(E(Y))}\right], \tag{7.43}$$

where $g_i(E(X))$ is the instantaneous estimator for the density of states of walker i at energy $E(X)$. Note that if the energy of one walker lies outside the energy range of the other sub-window, no exchange can occur.

Note that in this formalism, every walker is furnished with *its own* $g(E)$ and $H(E)$, which are updated independently. Also, every walker has to fulfill the flatness criterion *independently*, at each iteration, ensuring that systematic errors cannot occur. When every random walker within an energy sub-window has attained a flat histogram, the estimators for $g(E)$ are averaged out and redistributed among themselves before simultaneously proceeding to the next iteration. This practice reduces the error during the simulation as $m^{1/2}$, i.e. as for uncorrelated Wang–Landau simulations. Furthermore, increasing m can improve the convergence by reducing the risk of statistical outliers in $g(E)$ resulting in slowing down subsequent iterations. (Alternatively, it allows us, in principle, to use a weaker flatness criterion, which is in the spirit of a concurrently proposed idea of merging histograms in multicanonical simulations (Zierenberg *et al.*, 2013).) The simulation is terminated when all the energy intervals have attained f_{final}. At the end of the simulation, a total of $h \times m$ pieces of $g(E)$ fragments with overlapping energy intervals are used to calculate a single $g(E)$ in the complete energy range. The pieces are joined together where the inverse microcanonical temperatures (Schnabel *et al.*, 2011) coincide.

The acceleration in performance comes from two sources: (1) the replica exchange; and (2) the use of multiple cores. For modest numbers of cores, the speed-up can actually be super-linear, i.e. the improvement in performance can increase by a factor that is *greater* than the number of cores used. As an

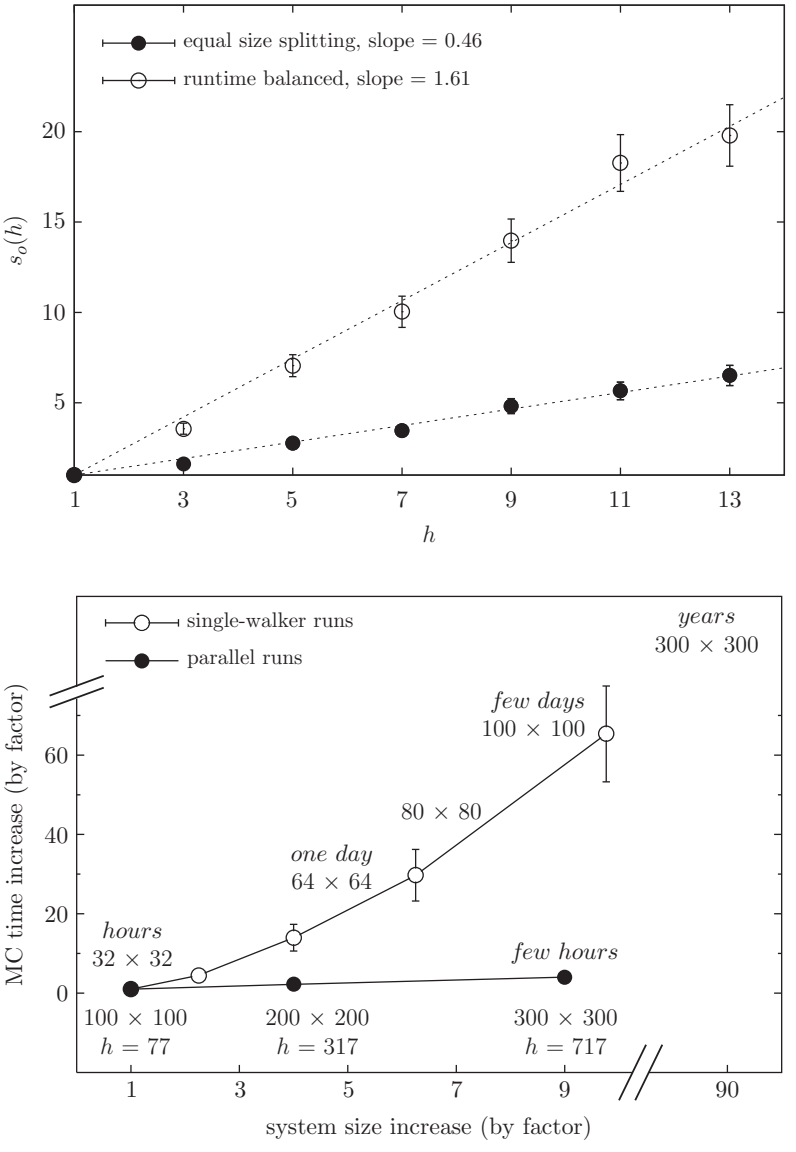

Fig. 7.13 Parallel speed-up of replica exchange Wang–Landau simulations for the $q = 10$ Potts model. From Vogel *et al.* (2014).

example of the improvement in performance we show results for the $q = 10$ Potts model in two dimensions in Fig. 7.13.

In Fig. 7.13 we see that larger systems can be studied with more cores in the same amount of 'wall clock time' (weak scaling), or a linear speed-up can be achieved by increasing the number of energy sub-intervals and thus the number of cores (strong scaling). Almost perfect scaling has already been demonstrated using several thousand cores, but there is no reason why this cannot be extended

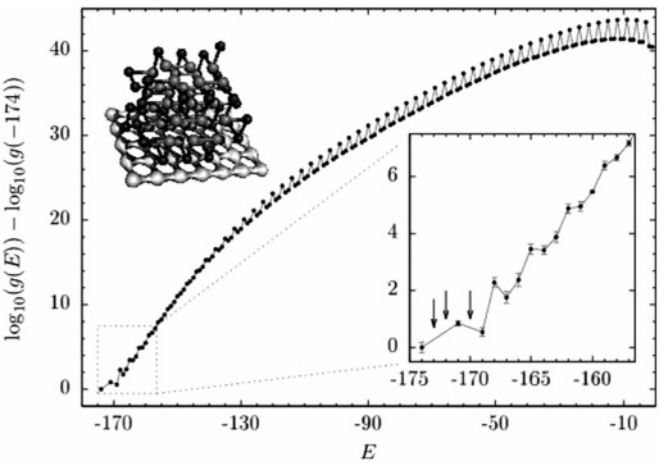

Fig. 7.14 Density of states for a 67mer HP lattice protein in the presence of a surface that attracts the Hmers only. The H-H interaction is three times stronger than the surface attraction. The picture shows an adsorbed HP protein with the groundstate energy. From Vogel *et al.* (2013).

by many more orders of magnitude using the same framework. The algorithm has been verified for both lattice models with discrete variables and for models in the continuum.

The improvement in performance allows the study of systems that are too complex for scalar runs. In Fig. 7.14 we show the density of states found for a 67mer HP model lattice protein in the presence of an attractive surface. Here the competition between hydrophobic core formation due to protein folding and protein surface adsorption means that the combination of a complex energy landscape and complicated entropic entanglements leads to an almost 'schizophrenic' sawtooth-like density of states. At first glance this result certainly looks like it is the result of an error in the computer program, but it is correct and cannot be obtained using standard methodology.

7.9 A CASE STUDY: EVAPORATION/CONDENSATION TRANSITION OF DROPLETS

We conclude this chapter with another case study that brings together multiple techniques of both simulation and analysis. The goal of this study is to determine the existence of an evaporation/condensation transition of a liquid droplet in a compressible, off-lattice fluid (MacDowell *et al.*, 2004). For this purpose a simple Lennard–Jones model (see Eqn. (6.4)) in three dimensions was used with interactions that were truncated at a cutoff radius r_c and shifted so as to eliminate discontinuities in the force at r_c. Fully periodic boundary conditions were imposed. Trial Monte Carlo moves included both particle insertions/deletions and particle moves. The probability $P(N)$ of finding N particles within the simulation cell was determined using Wang–Landau sampling (see Section 7.8). Typically the total range of states was subdivided

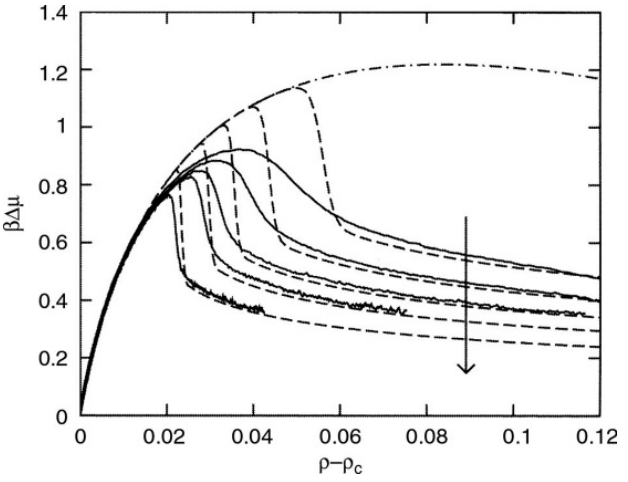

Fig. 7.15 Size dependence of the chemical potential–density loops for finite, Lennard–Jones systems. The volume size for each curve increases as the curves are displaced downward, as indicated by the arrow. Size range from $L = 11.3$ to $L = 22.5$. Solid curves are simulation data, while broken curves result from a phenomenological, theoretical description, and the dash-dotted curve represents the corresponding homogeneous phase. After MacDowell *et al*. (2004).

into windows, and simulations within a window were carried out independently and then linked together; however, near an evaporation transition a two-dimensional random walk within a single window in both n and E space proved to be most effective. In this way it was possible to obtain reliable, precise data; however, the analysis turned out to be somewhat subtle and yielded rather intriguing results. The finite size, i.e. N-particle, equation of state as a function of the chemical potential μ and particle number N was determined using

$$\frac{d \ln P(N)}{d N} = \mu(N) - \mu \tag{7.44}$$

where μ is the chemical potential imposed during the simulation. Quite pronounced 'van der Waals-type loops' were found, but these shifted systematically towards coexistence densities as the size increased, as can be seen in Fig. 7.15.

Unlike in mean field theory, those states to the left of the effective spinodal density are stable since they have a lower free energy than an inhomogeneous state with the same number of particles. Correspondingly, to the right of the effective spinodal density a stable, spherical droplet will coexist with the vapor. The effective spinodal density converges to the macroscopic coexistence value only in the limit $L \to \infty$, and in this limit $\Delta\mu = 0$ for all $\rho > \rho_c$, up to the liquid density, of course (the difference between the spinodal density and the coexistence density scales as $L^{-3/4}$). This figure shows that in the presence of phase coexistence, finite size effects involving unexpected subtleties occur.

REFERENCES

Adler, J. (1983), *J. Phys. A* **16**, 3585.

Baillie, C. F., Gupta, R., Hawick, K. A., and Pawley, G. S. (1992), *Phys. Rev. B* **45**, 10438.

Bennett, C. H. (1976), *J. Comput. Phys.* **22**, 245.

Berg, B. A. (1996), *J. Stat. Phys.* **82**, 343.

Berg, B. A. (1997), in *Proceedings of the International Conference on Multiscale Phenomena and Their Simulations* (Bielefeld, Oct. 1996), eds. F. Karsch, B. Monien and H. Satz (World Scientific, Singapore).

Berg, B. A., Hansmann, U., and Neuhaus, T. (1993), *Phys. Rev. B* **47**, 497.

Berg, B. and Neuhaus, T. (1991), *Phys. Lett. B* **267**, 249.

Berg, B. and Neuhaus, T. (1992), *Phys. Rev. Lett.* **68**, 9.

Binder, K. (1982), *Phys. Rev. A* **25**, 1699.

Binder, K. and Hohenberg, P. C. (1972), *Phys. Rev. B* **6**, 3461.

Binder, K. and Hohenberg, P. C. (1974), *Phys. Rev. B* **9**, 2194.

Binder, K. and Landau, D. P. (1984), *Phys. Rev. Lett.* **52**, 318.

Binder, K. and Luijten, E. (2001), *Physics Reports* **344**, 179.

Blöte, H. W. J. and Kamieniarz, G. (1993), J 196, 455.

Blöte, H. W. J., Compagner, A., Croockewit, J. H., Fonk, Y. T. J. C., Heringa, J. R., Hoogland, A., Smit, T. S., and van Willigen, A. L. (1989a), *Physica A* **161**, 1.

Blöte, H. W. J., de Bruin, J., Compagner, A., Croockewit, J. H., Fonk, Y. T. J. C., Heringa, J. R., Hoogland, A., and van Willigen, A. L. (1989b), *Europhys. Lett.* **10**, 105.

Blöte, H. W. J., Luijten, E., and Heringa, J. R. (1995), *J. Phys. A* **28**, 6289.

Butera, P. and Comi, M. (1997), *Phys. Rev. B* **56**, 8212.

Chen, K., Ferrenberg, A. M., and Landau, D. P. (1993), *Phys. Rev. B* **48**, 239.

Dayal, P., Trebst, S., Wessel, S., Wurtz, D., Troyer, M., Sabhapandit, S., and Coppersmith, S. N. (2004), *Phys. Rev. Lett.* **92**, 097201.

de Oliveira, P. M. C., Penna, T. J. P., and Herrmann, H. J. (1996), *Braz. J. Phys.* **26**, 677.

Deng, Y., Blöte, H. W. J., and Nightingale, M. P. (2005), *Phys. Rev. E* **72**, 018128.

Diehl, H. W. and Dietrich, S. (1981), *Phys. Rev. B* **24**, 2878.

Diehl, H. W. and Shpot, M. (1994), *Phys. Rev. Lett.* **73**, 3431.

Diehl, H. W. and Shpot, M. (1998), *Nucl. Phys. B* **528**, 469.

Ferrenberg, A. M. (1991), in *Computer Simulation Studies in Condensed Matter Physics III*, eds. D. P. Landau, K. K. Mon and H.-B. Schüttler (Springer-Verlag, Heidelberg).

Ferrenberg, A. M. and Landau, D. P. (1991), *Phys. Rev. B* **44**, 5081.

Ferrenberg, A. M. and Swendsen, R. H. (1988), *Phys. Rev. Lett.* **61**, 2635.

Ferrenberg, A. M. and Swendsen, R. H. (1989), *Phys. Rev. Lett.* **63**, 1195.

Fisher, M. E. (1995), *J. Phys. A* **28**, 6323.

Frenkel, D. and Smit, B. (1996), *Understanding Molecular Simulation: From Algorithms to Applications* (Academic Press, New York).

Hasenbusch, M. (2010), *Phys. Rev. B* **82**, 174433.

Hasenbusch, M. (2011), *Phys. Rev. B* **84**, 134405.

Hukusima, K. and Nemoto, K. (1996), *J. Phys. Soc. Japan* **65**, 1604.

Jain, T. S. and de Pablo, J. J. (2002), *J. Chem. Phys.* **116**, 7238.

Jain, T. S. and de Pablo, J. J. (2003), *J. Chem. Phys.* **118**, 4226.

Janke, W. (1992), in *Dynamics of First Order Transitions*, eds. H. J. Herrmann, W. Janke, and F. Karsch (World Scientific, Singapore).

Janke, W. (1997), in *New Directions in Statistical Physics*, eds. C.-K. Hu and K.-T. Leung (Elsevier, Amsterdam), p. 164.

Janke, W. and Kappler, S. (1995), *Phys. Rev. Lett.* **74**, 212.
Koller, W., Prull, A., and Evertz, H. G. (2003), *Phys. Rev. B* **67**, 104432.
Krech, M. and Landau, D. P. (1996), *Phys. Rev. E* **53**, 4414.
Landau, D. P. and Binder, K. (1990), *Phys. Rev. B* **41**, 4633.
Lee, Y. and Choi, M. Y. (1994), *Phys. Rev. E* **50**, 4420.
LeGuillou, J.-C. and Zinn-Justin, J. (1980), *Phys. Rev. B* **21**, 3976.
Li, Y.-W., Wüst, T., Landau, D. P., and Lin, H.-Q. (2007), *Comp. Phys. Commun.* **177**, 524.
Liu A. J. and Fisher, M. E. (1989), *Physica A* **156**, 35.
Liu, A. and Fisher, M. E. (1990), *J. Stat. Phys.* **58**, 431.
Livet, F. (1991), *Europhys. Lett.* **16**, 139.
Lyubartsev, A. P., Martsinovski, A. A., Shevkunov, S. V., and Vorentsov-Velyaminov, P. N. (1992), *J. Chem. Phys.* **96**, 1776.
MacDowell, L. G., Virnau, P., Müller, M., and Binder, K. (2004), *J. Chem. Phys.* **120**, 5293.
Marinari, E. and Parisi, G. (1992), *Europhys. Lett.* **19**, 451.
Mognetti, B. M., Yelash, L., Virnau, P., Paul, W., Binder, K., Müller, M., and MacDowell, L. G. (2008), *J. Chem. Phys.* **128**, 104501.
Mon, K. K. (1985), *Phys. Rev. Lett.* **54**, 2671.
Müller, M. and de Pablo, J. J. (2006), in *Computer Simulations in Condensed Matter: From Materials to Chemical Biology*, eds. M. Ferrario, G. Ciccotti, and K. Binder (Springer, Heidelberg), vol. 1, p. 67.
Müller, M., Binder, K., and Oed, W. (1995), *J. Chem. Soc. Faraday Trans.* **28**, 8639.
Nickel, B. G. and Rehr, J. J. (1990), *J. Stat. Phys.* **61**, 11.
Nightingale, M. P. and Blöte, H. W. J. (1988), *Phys. Rev. Lett.* **60**, 1662.
Novotny, M. A. (1991), *Nucl. Phys. B Proc. Suppl.* **20**, 122.
Pawley, G. S., Swendsen, R. H., Wallace, D. J., and Wilson, K. G. (1984), *Phys. Rev. B* **29**, 4030.
Pelissetto, A. and Vicari, E. (2002), *Phys. Rep.* **368**, 549.
Rathore, N., Knotts, T. A., and de Pablo, J. J. (2003), *J. Chem. Phys.* **118**, 4285.
Reuhl, M. (1997), Diplomarbeit (University of Mainz, unpublished).
Rosengren, A. (1986), *J. Phys. A* **19**, 1709.
Ruge, C., Dunkelmann, S., and Wagner, F. (1992), *Phys. Rev. Lett.* **69**, 2465.
Saito, M. and Matsumoto, H. (2009), in *Monte Carlo and Quasi-Monte-Carlo Methods 2006*, ed. A. Keller, S. Heinrich, and H. Niederreiter (Springer, Berlin).
Salman, Z. and Adler, J. (1998), *Int. J. Mod. Phys. C* **9**, 195.
Schnabel, S., Seaton, D. T., Landau, D. P., and Bachmann, M. (2011), *Phys. Rev. E* **84**, 011127.
Schulz, B. J., Binder, K., and Mueller, M. (2002), *Int. J. Mod. Phys. C* **13**, 477.
Schulz, B. J., Binder, K., Mueller, M., and Landau, D. P. (2003), *Phys. Rev. E* **67**, 067102.
Shell, M. S., Debenedetti, P. G., and Panagiotopoulos, A. Z. (2002), *Phys. Rev. E* **66**, 056703.
Shing, K. S. and Gubbins, K. E. (1983), *Mol. Phys.* **49**, 1121.
Torrie, G. M. and Valleau, J. P. (1977), *J. Comput. Phys.* **23**, 187.
Tröster, A. and Dellago, C. (2005), *Phys. Rev. E* **71**, 066705.
Troyer, M., Sabhapandit, S., and Coppersmith, S. N. (2003), *Phys. Rev. Lett.* **92**, 097201.
Troyer, M., Wessel, S., and Alet, F. (2003), *Phys. Rev. Lett.* **90**, 120201.
Tsai, S.-H., Wang, F., and Landau, D. P. (2007), *Phys. Rev. E* **75**, 061108.
Vendruscolo, M., Rovere, M., and Fasolino, A. (1992), *Europhys. Lett.* **20**, 547.

Virnau, P. and Muller, M. (2004), *J. Chem. Phys.* **120**, 10925.
Vogel, V., Li, Y. W., Wüst, T., and Landau, D. P. (2013), *Phys. Rev. Lett.* **110**, 210603.
Vogel, V., Li, Y. W., Wüst, T., and Landau, D. P. (2014), *Phys. Rev. E* **90**, 023302.
Wang, F. and Landau, D. P. (2001), *Phys. Rev. Lett.* **86**, 2050; *Phys. Rev. E* **64**, 056101.
Wang, J.-S., Tay, T. K. and Swendsen, R. H. (1999), *Phys. Rev. Lett.* **82**, 476.
Wansleben, S. and Landau, D. P. (1991), *Phys. Rev. B* **43**, 6006.
Yamaguchi, C. and Kawashima, N. (2002), *Phys. Rev. E* **65**, 056710.
Yan, Q. and de Pablo, J. J. (2003), *Phys. Rev. Lett.* **90**, 035701.
Yin, J. and Landau, D. P. (2012), *Comput. Phys. Commun.* **183**, 1568.
Zhou, C. and Bhatt, R. H. (2005), *Phys. Rev. E* **72**, 025701.
Zhou, C., Schulthess, T. C., Torbrügge, S., and Landau, D. P. (2006), *Phys. Rev. Lett.* **96**, 120201.
Zierenberg, J., Marenz, M., and Janke, W. (2013), *Comput. Phys. Commun.* **184**, 1155.
Zinn-Justin, J. (2001), *Physics Reports* **344**, 159.